Redox Biology 58 (2022) 102537

Contents lists available at ScienceDirect

Redox Biology

journal homepage: www.elsevier.com/locate/redox

Ablation of Shank3 alleviates cardiac dysfunction in aging mice by promoting CaMKII activation and Parkin-mediated mitophagy☆

Ying Wang [a], Yuerong Xu [b], Wangang Guo [a], Yexian Fang [a], Lang Hu [a], Runze Wang [a], Ran Zhao [a], Dong Guo [a], Bingchao Qi [a], Gaotong Ren [a], Jun Ren [c,**], Yan Li [a,***], Mingming Zhang [a,*]

[a] Department of Cardiology, Tangdu Hospital, Air Force Medical University, Xi'an, 710038, China
[b] Department of Orthodontics, School of Stomatology, Air Force Medical University, Xi'an, 710032, China
[c] Department of Cardiology and Shanghai Institute of Cardiovascular Diseases, Zhongshan Hospital, Fudan University, Shanghai, China

ARTICLE INFO

Keywords:
Cardiac aging
Mitophagy
Shank3
CaMKII
Oxidative stress

ABSTRACT

Compromised mitophagy and mitochondrial homeostasis are major contributors for the etiology of cardiac aging, although the precise underlying mechanisms remains elusive. Shank3, a heart-enriched protein, has recently been reported to regulate aging-related neurodegenerative diseases. This study aimed to examine the role of Shank3 in the pathogenesis of cardiac senescence and the possible mechanisms involved. Cardiac-specific conditional Shank3 knockout ($Shank3^{CKO}$) mice were subjected to natural aging. Mitochondrial function and mitophagy activity were determined *in vivo*, in mouse hearts and *in vitro*, in cardiomyocytes. Here, we showed that cardiac Shank3 expression exhibited a gradual increase during the natural progression of the aging, accompanied by overtly decreased mitophagy activity and a decline in cardiac function. Ablation of Shank3 promoted mitophagy, reduced mitochondria-derived superoxide (H_2O_2 and $O_2\bullet^-$) production and apoptosis, and protected against cardiac dysfunction in the aged heart. In an *in vitro* study, senescent cardiomyocytes treated with D-gal exhibited reduced mitophagy and significantly elevated Shank3 expression. Shank3 knock-down restored mitophagy, leading to increased mitochondrial membrane potential, decreased mitochondrial oxidative stress, and reduced apoptosis in senescent cardiomyocytes, whereas Shank3 overexpression mimicked D-gal-induced mitophagy inhibition and mitochondrial dysfunction in normally cultured cardiomyocytes. Mechanistically, the IP assay revealed that Shank3 directly binds to CaMKII, and this interaction was further increased in the aged heart. Enhanced Shank3/CaMKII binding impedes mitochondrial translocation of CaMKII, resulting in the inhibition of parkin-mediated mitophagy, which ultimately leads to mitochondrial dysfunction and cardiac damage in the aged heart. Our study identified Shank3 as a novel contributor to aging-related cardiac damage. Manipulating Shank3/CaMKII-induced mitophagy inhibition could thus be an optional strategy for therapeutic intervention in clinical aging-related cardiac dysfunctions.

1. Introduction

Cardiovascular diseases (CVDs) are among the leading causes of morbidity and mortality worldwide, despite major advances in CVD therapeutics over the last decades [1]. Aging is an independent risk factor for CVDs, given that the majority of CVDs develop in patients aged 60 years or higher. Various CVDs account for 40% of all-cause mortality among the elderly [2]. However, effective strategies for the management of CVDs have been suboptimal in the elderly population. Accumulating clinical and experimental evidence has revealed that biological aging process is often associated with organelle dysfunction, ultimately leading to oxidative stress, inflammation, and cell death [3,4]. For example, compromised mitochondrial homeostasis is considered an important pathological feature of aging hearts in both human and animal models [5,6]. Mitochondria produce over 90% of the ATP utilized for cell energy metabolism. Mitochondria serve as the primary

☆ Ying Wang, Yuerong Xu and Wangang Guo contributed equally to this work.

* Corresponding author.
** Corresponding author. Department of Cardiology and Shanghai Institute of Cardiovascular Diseases, Zhongshan Hospital, Fudan University, Shanghai, China.
*** Corresponding author.
E-mail addresses: jren@uw.edu (J. Ren), profleeyan@163.com (Y. Li), winterzhang3@163.com (M. Zhang).

https://doi.org/10.1016/j.redox.2022.102537
Received 31 October 2022; Accepted 8 November 2022
Available online 18 November 2022

organelles for reactive oxygen species (ROS) production in cardiomyocytes [7]. Cardiac aging is accompanied by a decline in mitochondrial function, accumulation of dysfunctional mitochondria, increased ROS production, and dysregulated mitochondrial quality control [8,9]. Damaged mitochondria cannot be easily cleared away via cell division, given their insufficient ability to proliferate and dilute damaged mitochondria through cell division. Instead, adult hearts are mainly dependent on the proper functioning of mitochondrial quality control mechanisms to retard mitochondria-related pathologies in the aging process [10].

Mitophagy, a form of selective autophagy for mitochondria predominantly through the PINK1/Parkin-mediated ubiquitin-dependent pathway, serves as an important machinery to eliminate damaged mitochondria and maintain cellular mitochondrial homeostasis [11]. Dysregulated mitophagy is commonly seen in cardiovascular pathologies, including cardiac hypertrophy, heart failure and dilated cardiomyopathy [12,13]. Downregulation of mitophagy has been reported to contribute to the organ aging process [14–16]. Notably, defective mitophagy is commonly observed in aging cardiomyocytes, which leads to the accumulation of defective mitochondria. For example, PINK1 suppression is an important feature of aging-related diseases [17], whereas parkin deficiency evokes distorted mitochondria and cardiac aging [18]. In contrast, parkin over-expression has been reported to promote the renewal of damaged mitochondria by inducing mitochondrial fission, and retarding aging [19]. Induction of mitophagy in aging mouse hearts by promoting the incorporation of defective mitochondria into autophagosomes alleviates aging-related decline in cardiac function [18]. Moreover, oral administration of the natural polyamine spermidine was found to alleviate cardiac hypertrophy, and preserve cardiac function by promoting mitochondrial respiration and mitophagy in cardiomyocytes [20]. These preclinical studies have convincingly suggested a crucial role of dampened mitophagy in the pathogenesis of cardiac aging, indicating the promises of interventions targeting mitophagy in cardiac aging. However, specific strategies for manipulating PINK1/Parkin-mediated mitophagy in aging hearts remain undefined, prompting the search for new therapeutic mitophagy-related strategies in the elderly.

SHANK, which is localized at excitatory synapses, functions as a scaffolding protein to tether and organize intermediate scaffolding proteins [21]. Shank proteins are encoded by Shank1, Shank2, and Shank3, of which Shank3 is the most widely studied in neurological disorders [22]. Previous studies have shown a vital role for Shank3 in the dynamic regulation of postsynaptic receptors and signaling molecules through protein targeting and anchoring [23]. Shank3 is involved in multiple physiological processes by directly or indirectly interacting with various proteins, including cell adhesion proteins, cytoskeletal proteins, and metabotropic glutamate receptors (mGluRs) [24]. Mutations in Shank3 are strongly associated with a high incidence of aging-related neurodegenerative diseases, including Parkinson's diseases and Alzheimer's diseases [25]. Mechanistically, neural stem cells from Shank3 knockout mice exhibited inhibited autophagy, indicating a close correlation between Shank3 and autophagy in the nervous system [26]. In the cardiovascular system, Shank3 is confirmed to be highly expressed in the heart [27] and is involved in the pathological development of CVDs. Sarcolemma-localized Shank3 promotes hypertrophic responses in cardiomyocytes, while Shank3 knockdown alleviates myocardial hypertrophic growth [28]. Considering the emerging role of Shank3 in CVDs and aging-related diseases, it is essential to elucidate its role of Shank3 in cardiac aging, especially from the perspective of mitophagy loss and mitochondrial dysfunction.

The major finding from this study indicated a role for upregulated Shank3 in the suppression of mitophagy and mitochondrial function in aging hearts. Moreover, ablation of Shank3 effectively restored mitophagy, leading to preserved mitochondrial function, decreased mitochondrial oxidative stress, and consequently improved cardiac function. Mechanistically, Shank3 directly binds to CaMKII to impede its mitochondrial translocation, which further inhibits CaMKII activation and parkin-mediated mitophagy. These findings suggest the promises of Shank3-induced inhibition of mitophagy as a target for therapeutic intervention in cardiac aging.

2. Method

2.1. Animal experiments

All animal experiments were approved by the Animal Use and Care Committee of the Air Force Medical University. In order to avoid the potential effect of female hormone changes on cardiac function and cardiomyocytes function during natural aging process, female mice were excluded in this study [29]. The floxed-Shank3 mice were developed by Jackson Laboratory (Bar Harbor, ME, USA). Mice expressing the cardiac α-myosin heavy chain (αMyHC)-Cre recombinase were purchased from Jackson Laboratory (Bar Harbor, ME, USA). Male cardiac-specific Shank3 knockout ($Shank3^{f/f}Cre^{+/-}$, $Shank3^{CKO}$) mice were generated by crossing female $Shank3^{wt/f}Cre^{\pm}$ mice with male $Shank3^{wt/f}Cre^{\pm}$ mice. Littermate male $Shank3^{f/f}$ mice were used as control mice. To induce Cre expression, tamoxifen (Sigma) was injected intraperitoneally for mice once a day for 4–6 days at a dose of 20 mg/kg/day from 4-weeks of age. All mice were housed in temperature-controlled cages with a 12 h light-dark cycle and free access to water and food. Cardiac-specific conditional Shank3 knockout ($Shank3^{CKO}$) murine models and their control littermates ($Shank3^{f/f}$) were subjected to chow diet feeding for 18 months as a natural biological aging model.

2.2. Echocardiography

To determine the cardiac function of mice, an M-mode echocardiography device (Vevo 2100; Visual Sonics, Toronto, ON, Canada) was used as previously described [30]. The heart rate of the mice was monitored using a real-time ECG monitoring system during echocardiography. Mice were anesthetized with 2.5% isoflurane, and M-mode echocardiographic images were recorded. Left ventricular ejection fraction (LVEF) and left ventricular fractional shortening (LVFS) were analyzed using computer algorithms.

2.3. Wheat germ agglutinin (WGA) staining

WGA staining was performed using a wheat germ agglutinin conjugate (Green, Thermo Fisher Scientific, United States) as previously described [31]. Images were captured using an EVOS M5000 fluorescence microscope (Thermo Fisher Scientific, USA). The cross-sectional area was calculated using ImageJ software by a technician who was blinded to the study. At least 300 cardiomyocytes from a minimum of 6 images per group were analyzed.

2.4. Histological analysis

For histological analysis, mouse hearts were collected and fixed overnight in 4% paraformaldehyde (PH7.4) overnight. A Masson staining kit (Solarbio Life Sciences, China) was used to detect intramyocardial collagen content according to the manufacturer's instructions [32].

2.5. Dihydroethidium (DHE) staining

DHE staining was performed to determine intracellular superoxide anion ($O_2\bullet^-$) levels in mice hearts. Images were obtained using an EVOS M5000 Imaging System (Thermo Fisher, USA). Image-Pro Plus image analysis software was used to analyze the images.

2.6. Detection of manganese superoxide dismutase (MnSOD) and malondialdehyde (MDA) levels in mice heart

MnSOD activity and MDA levels were detected according to the manufacture's instruction using Mn-SOD Assay Kits (S0103, Beyotime Biotechnology, Jiangsu, China) and lipid peroxidation MDA assay kits (S0131, Beyotime Biotechnology, Jiangsu, China).

2.7. Determination of measurement of H_2O_2 production in isolated heart mitochondria

To measure H_2O_2 production, mitochondria were isolated from mice hearts with a Tissue Mitochondria Isolation Kit (Beyotime Biotechnology, Jiangsu, China) and then stained with a 10 μM H_2O_2-sensitive dye Amplex red reagent (Thermo Fisher, Waltham, MA) [32]. A Bio-Tek plate reader was used to record the fluorescence density every 3 min for a total of 30 min H_2O_2 production was calculated using linear regressions.

2.8. Detection of protein carbonylation

To detect protein carbonylation in the heart tissue of mice, an anti-DNPH antibody (OxyBlot™ Protein Oxidation Detection Kit, Merck Millipore, Darmstadt, Germany) and a Coomassie Brilliant Blue R assay (Sigma) were used following a general protocol. Briefly, the cardiac tissue was lysed in lysis buffer. Tissue proteins were extracted and then loaded onto two sodium dodecyl sulfate-polyacrylamide gel electrophoresis gels. Thereafter, one gel was stained with Coomassie Brilliant Blue (CBB) to analyze the protein on the gel, and another gel was electroblotted and transferred to the membrane according to the standard protocol. The membrane was blocked with blocking buffer and incubated with anti-DNPH antibody. Protein carbonylation levels were measured by normalizing blot-signals with Coomassie blue signals.

2.9. Apoptosis assay

To determined apoptosis in mice hearts and cultured cardiomyocytes, a terminal deoxynucleotidyl transferase UTP nick end labelling (TUNEL) assay kit (Roche Applied Science, Switzerland) was used *in vivo*, whereas a PE-Annexin V Apoptosis Detection Kit (BD Science) was used *in vitro*. All procedures were conducted strictly according to the manufacturer's instructions as previously described [33].

2.10. Transmission electronic microscopy (TEM)

For TEM detection, heart samples were trimmed into smaller pieces and fixed with 2% glutaraldehyde, as previously described [34]. Images were obtained using a TEM (JEM-1230; JEOL Ltd., Tokyo, Japan) at 300 kV. The TEM images were analyzed using Image Pro Plus software by an experienced technician blinded to the treatment. Intracellular double-membrane vesicles containing mitochondria were identified as mitochondrial-autophagosomes, which reflect the level of mitophagy activity in heart samples. The number of mitochondrial autophagosomes was calculated in an area larger than 1200 μm^2 in six images per group.

2.11. Primary neonatal rat cardiomyocytes isolation and culture

Primary neonatal cardiomyocytes were prepared from neonatal rat hearts (aged 0–3 days old). Thereafter, the cardiomyocytes were treated with D-galactose (Sigma, USA) dissolved in medium and incubated for 48 h.

2.12. Senescence-associated β-galactosidase staining

Senescence-associated β-galactosidase staining was performed according to the manufacturer's protocol [35]. Briefly, cardiomyocytes were fixed and then incubated with a β-galactosidase staining solution for 24 h. Images were obtained using a an EVOS M5000 imaging system (Thermo Fisher, USA). The percentage of blue-stained cells was calculated to assess cellular senescence.

2.13. Mitochondrial membrane potential (MMP) determination

For MMP determination, a JC-1 Mitochondrial Membrane Potential assay kit (Abcam, Cambridge, UK) was used following the manufacturer's protocol [36]. Briefly, cardiomyocytes were seeded in a 20 mm-culture dish with a clear bottom. JC-1 staining was used to calculate MMP as the ratio of fluorescence of red (JC-1 polymer) to green (JC-1 monomer) fluorescence.

2.14. Determination of superoxide anion in mitochondria of primary cardiomyocytes

Mito-Sox Red staining (Invitrogen, USA) was used to detect the mitochondrial superoxide anion [37]. Mito-Sox Red staining (Invitrogen, USA) was used to detect mitochondrial superoxide anions. Images were obtained using a confocal laser scanning microscope (Nikon, A1R, Japan).

2.15. Adenovirus transfection

Primary neonatal cardiomyocytes were transfected with an adenovirus harboring Shank3 (Ad-Shank3), CaMKII (Ad-CaMKII), or Shank3 shRNA (Ad-sh-Shank3). The cells were treated with normal medium for 24 h after adenovirus transfection.

2.16. Assessment of mitophagy and autophagy in cells

Mitochondria were labeled with a MitoTracker Red CMXRos probe (Thermo Fisher, USA). Cell cytoskeleton and morphology were evaluated by staining with phalloidin. To label LC3, cardiomyocytes were transfected with an adenovirus harboring GFP-LC3. Mitophagy was detected by colocalization of GFP-LC3 with the mitochondria and cytoskeleton. The fluorescence images were obtained using a Nikon A1R laser confocal microscope [38].

2.17. Co-immunoprecipitation (Co-IP)

Co-IP assays for protein-protein interactions were conducted using an IP/Co-IP kit (Thermo Fisher, USA) according to the manufacturer's instructions [39]. Briefly, for IP experiments, cell lysates were incubated overnight with the primary antibody for immunoprecipitation at 4 °C. Protein A/G magnetic beads were added and allowed to bind to the antigen/antibody complex for 2 h at room temperature. Protein samples containing dithiothreitol were heated and separated by electrophoresis. The proteins samples were immunoblotted and incubated with primary antibodies to verify the efficiency of immunoprecipitation.

2.18. Immunofluorescence

Overlap of CaMKII with Shank3 or MitoTracker immunofluorescence was performed as per the standard immunofluorescence protocol, and staining was performed as previously described [40]. For colocalization in the fluorescence images, the resulting images were analyzed using the EzColocalization plugin for the ImageJ image analysis software as reported by Stauffer, W. et al. [41] The Pearson colocalization coefficient for different signals was calculated by a researcher blinded to the treatment.

2.19. Western blotting

Western blotting was performed as previously described [42]. The

primary antibody for the following protein were used: GAPDH (Cell signaling technology, #51332), β-actin (Abcam, #ab8227), Shank3 (Abcam, #ab264347), Nox4 (Abcam, #ab13303), cleaved-capase9 (Abcam, #ab184786), PINK1(Abcam, #ab23707), Parkin (Abcam, #ab77924), *p*-Parkin (Cell signaling technology, #36866), LC3 (Cell signaling technology, #4108), P62 (Abcam, #ab91526), Beclin1 (Abcam, #ab62557), Bax (Abcam, #ab53154), Bcl-2 (Abcam, #ab59348), CaMKII (Cell signaling technology, #3362), P16 (Abcam, #ab151303), P21(Abcam, #ab109199), P53 (Abcam, #ab131442), PGC1-α (Abcam, #ab54481), TFAM (Cell signaling technology, #7495), NRF-1 (Abcam, #ab55744).

To detect protein levels in the mitochondrial fraction, cytosol, and total cell fractions, a mitochondria/cytosol kit (Beyotime, China) was used to isolate mitochondria and cytosol, according to the manufacturer's protocol. Each fraction was quantified using a protein quantitation kit. For western-blot analysis, each fraction was loaded based on equal protein quantity (30 μg) and Western blot analysis was performed. GAPDH served as a loading control for the total cell and cytosol fractions, whereas VDAC1 was used as a loading control for the mitochondrial fraction.

2.20. Statistical analysis

All experimental data were analyzed using GraphPad Prism8.0 software. The results are presented as Mean ± SEM. When comparing two groups, an unpaired 2-tailed Student's *t*-test was used, and multiple comparisons were analyzed using ANOVA with a Bonferroni post hoc test. The results were considered statistically significant at $P < 0.05$.

3. Results

3.1. Ablation of Shank3 alleviated cardiac dysfunction in aging mice

Levels of well-established senescence markers, including P16, P21, and P53, were determined in an 18-month biological aging model. As shown in Figs. 1A–D, senescence marker levels were higher in aged

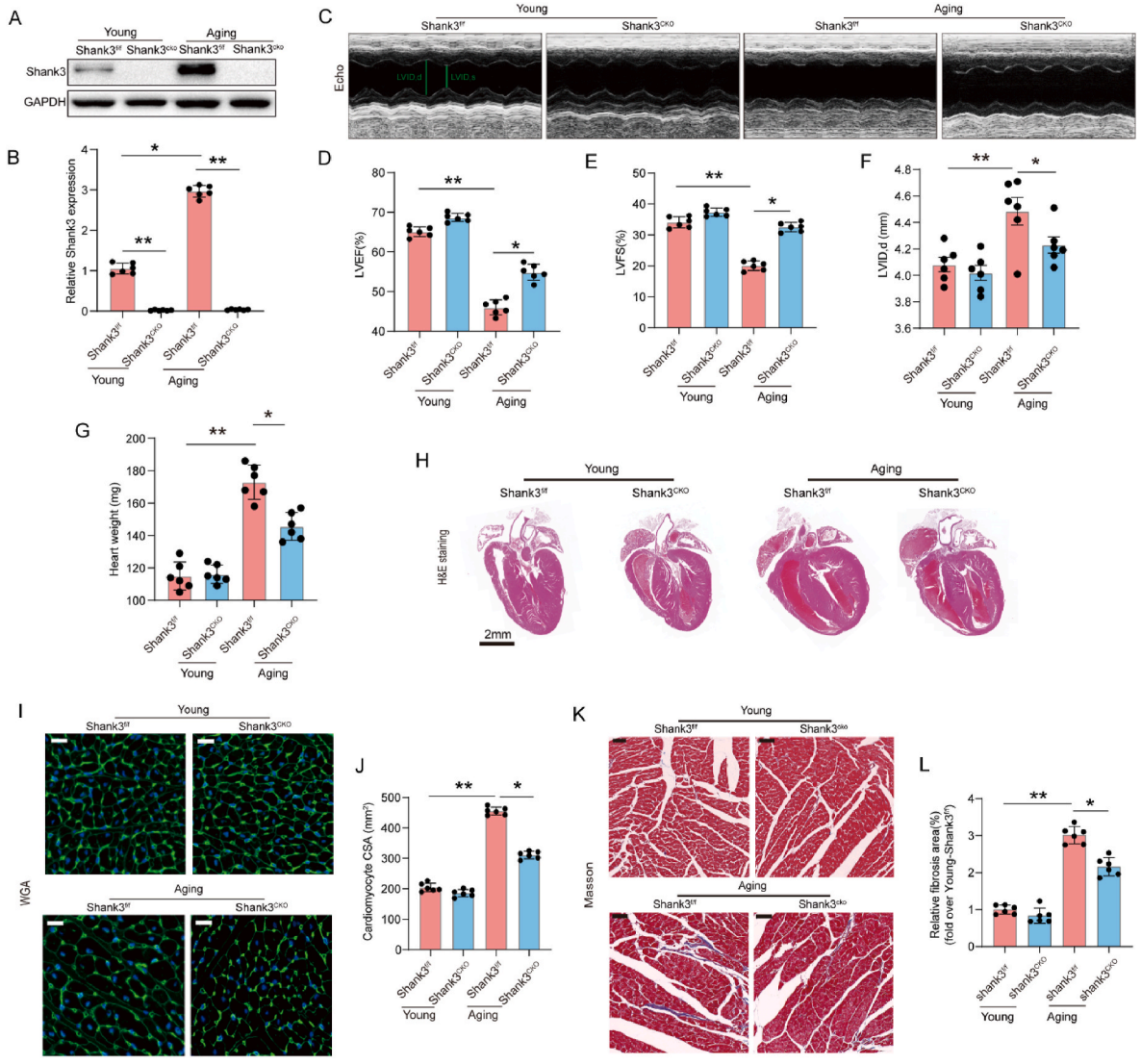

Fig. 1. Ablation of Shank3 protects against cardiac damage in aging mice. A&B Representative blot images and quantitative analysis of Shank3 expression in heart of young or aged mice (Mean ± SEM, n = 6 mice per group, *P<0.05, **P<0.01); **C** Representative echocardiographic images from young and aged mouse hearts; **D** Left ventricular ejection fraction (LVEF) (Mean ± SEM, **P<0.01); **E** Left ventricular fractional shortening (LVFS) (Mean ± SEM, **P<0.01); **F** Left ventricular end-diastolic internal diameter (LVID, d) (Mean ± SEM, *P<0.05, **P<0.01); **G** Heart weight. n = 6 mice per group; **H** Gross morphology of hearts stained by hematoxylin and eosin staining, Scale bar = 2 mm; **I&J** Representative images of WGA staining and quantitative analysis of cardiomyocyte CSA, Scale bar = 20 μm (Mean ± SEM, n = 6 images per group, *P<0.05, **P<0.01); **K** Representative images of Masson trichrome staining of hearts; and **L** Quantitative analysis of interstitial fibrosis. Scale bar = 50 μm (Mean ± SEM, n = 6 mice per group, *P<0.05, **P<0.01).

hearts than in young mice. To investigate whether Shank3 is involved in myocardial senescence, wild-type mice were allowed to age naturally, and Shank3 expression in cardiac tissue was determined at different time points. Interestingly, Shank3 expression was maintained at a low level from birth to early adulthood (1 day–6 months old). During late adulthood, Shank3 expression displayed a gradual increase as natural aging progressed (6–18 months old) (Fig. S1E). To explore the specific role of Shank3 in cardiac aging, a conditional cardiac-specific Shank3 knockout ($Shank3^{CKO}$) murine model was constructed and further validated by Western blot analysis (Fig. 1F). Both $Shank3^{CKO}$ mice and their control littermates ($Shank3^{f/f}$) were fed a chow diet for 18-months. As shown in Fig. 1A and B, after feeding for 18 months, Shank3 expression was significantly higher in aged-$Shank3^{f/f}$ mouse hearts than in young mice. Cardiac function was assessed by echocardiography. As shown in Fig. 1C–F, reduced cardiac function and obvious cardiac remodeling were observed in aged $Shank3^{f/f}$ mice, as evidenced by decreases in LVEF and LVFS, and elevated left ventricular internal diameter in diastole (LVID, d). Shank3 ablation effectively alleviated cardiac dysfunction and cardiac remodeling in aging mice, as indicated by increased LVEF and LVFS and decreased LVID. Cardiac hypertrophy and fibrosis are the main features of cardiac aging. As shown in Fig. 1G-L, aged $Shank3^{f/f}$ mice displayed evident cardiac hypertrophy and fibrosis compared to adult $Shank3^{f/f}$ mice, indicated by heavier heart weight, enlarged heart, greater cardiomyocyte cross-sectional area, and increased interstitial fibrosis, all of which were efficiently ameliorated by Shank3 ablation (Fig. 1G–L). These data support a role for Shank3 upregulation in the development of cardiac senescence, whereas Shank3 knockout attenuates aging-induced cardiac dysfunction.

3.2. Shank3 ablation inhibited mitochondria-derived superoxide production and cardiomyocyte apoptosis in senescent hearts

Cardiac aging is usually accompanied by increased intra-cellular superoxide anion production, with Nox-4 being the major mediator [43]. Superoxide anion levels were detected in both young and aged hearts. As shown in Fig. 2A–D, intracellular superoxide anion production ($O_2\bullet^-$, stained by DHE) and myocardial Nox-4 levels were significantly increased in the aged heart. Protein oxidation products, such as carbonylated proteins and lipid peroxidation products, are also biological indicators of cardiac aging. As shown in Fig. 2E–G, cardiac tissue from aging mice had a significantly higher carbonylated protein and MDA level than young mice, while MnSOD, a well-established indicator of antioxidant activity, was obviously lower. In addition, heart mitochondria were isolated and H_2O_2 production in mitochondria was determined using the H_2O_2 sensitive dye Amplex Red reagent. As shown in Fig. 2H and I, mitochondria-derived H_2O_2 production was significantly higher in the hearts of aged-$Shank3^{f/f}$ mice. Ablation of Shank3 reduced mitochondria-derived superoxide production, as evidenced by decreased DHE fluorescence and Nox-4 levels, reduced mitochondrial H_2O_2 production, reduced protein oxidation products content and increased MnSOD activity (Fig. 2A–I). Increased mitochondria-derived superoxide production causes apoptosis in cardiomyocytes [44]. The cleaved caspase-9/caspase-9 ratio, and apoptotic nuclei detected using the TUNEL assay were used as indicators of cell apoptosis. Compared to hearts from control $Shank3^{f/f}$ mice, cleaved caspase-9 and TUNEL-positive cell rate were overtly increased in hearts from aged $Shank3^{f/f}$ mice, the effects of which were reversed following Shank3 knockout (Fig. 2J-M). Taken together, these data indicate that Shank3 ablation suppresses mitochondria-derived oxidative stress and reduces cardiomyocyte apoptosis in the aging hearts.

3.3. Ablation of Shank3 restored mitophagy in aged hearts and D-gal-induced senescent cardiomyocytes

Defective mitophagy is deemed a hallmark of senescent cardiomyocytes [45]. We wondered whether Shank3 was involved in mitophagy inhibition in aged hearts. As shown in Fig. 3A and B, TEM analysis revealed an overtly reduced abundance of mitophagosomes in the hearts of aged $Shank3^{f/f}$ mice, while ablation of Shank3 recovered the number of mitophagosomes in the aged heart. Interestingly, Shank3 ablation also decreased the percentage of mitochondria with disorganized cristae, indicating an improved mitochondrial function (Fig. 3C). Mitophagy activity was determined using western blotting. As shown in Fig. 3D–H, both mitophagy indicators (PINK1 and Parkin) and autophagy indicator (LC3II/LC3I) were significantly downregulated, while autophagy indicator (P62) was upregulated in aged $Shank3^{f/f}$ mice hearts. As expected, Shank3 ablation restored mitophagy and autophagy, as indicated by the elevation of both mitophagy and autophagy activity in aged $Shank3^{CKO}$ mice hearts. (Fig. 3D–H).

The effect of Shank3 on mitophagy activity was also determined in D-gal-treated neonatal rat cardiomyocytes. The D-gal-induced senescent cardiomyocyte model was validated by senescence-associated β-galactosidase (SA β-Gal) staining (Fig. 2 and 3). Consistent with our *in-vivo* results, D-gal treatment significantly increased Shank3 levels in neonatal cardiomyocytes, whereas mitophagy and autophagy activity were significantly decreased. Knockdown of Shank3 in D-gal-treated cardiomyocytes restored mitophagy and autophagy activity, as indicated by elevated PINK1, Parkin, Beclin1, and LC3II/LC3I ratios and decreased P62 expression (Fig. 3I-O). The translocation of LC3 from the cytoplasm to mitochondria is a key step in mitophagy. In this study, LC3 was labeled with GFP (green), and mitochondria were labeled with Mito-Tracker (red). As shown in Figure 3P&Q, co-localization of GFP-LC3 and mitochondria was significantly lower in D-gal-treated cardiomyocytes, indicating a suppressed mitophagy activity. Shank3 knockdown promotes the co-localization of LC3 and mitochondria in senescent cardiomyocytes. To further explore whether Shank3 ablation activates mitophagy by promoting autophagosome formation or autophagy flux, both 3-MA, an inhibitor of autophagosome formation, and bafilomycin A1, a classic inhibitor of autophagic flux, were used in senescent cardiomyocytes in the absence or presence of Shank3 ablation. As shown in Fig. S4, 3-MA mitigated Shank3 ablation-induced mitophagy activation, for that Shank3 knockdown failed to restore mitophagy indicators including PINK1, Parkin, LC3II/I ratio and mitochondrial-localized LC3 puncta in 3-MA-treated senescent cells. In contrast, the autophagic flux inhibitor Baf-A1 failed to eliminate the mitophagy activity restoration induced by Shank3 ablation, for that data showed Shank3 ablation leads to parallel increases of LC3II/I ratio and mitochondrial LC3 puncta in vehicle- and Baf-A1-treated cells (Fig. S4). These data suggested that, compared with autophagic flux, autophagosome formation plays a more dominant role in the restoration of mitophagy activity restored by Shank3 ablation. Elevated mitophagy has been reported to provide the starting material for the synthesis of new mitochondria [50]. To support this notion, mitochondrial biogenesis, which is reflected by the levels of PGC-1α, TFAM, and NRF-1, was also inhibited in senescent cardiomyocytes (Fig. 5), while Shank3 knockdown promoted mitochondrial biogenesis in D-gal-treated cardiomyocytes. These *in vivo* and *in vitro* results suggest that Shank3 knockout protects against aging-induced cardiac dysfunction by promoting mitophagy.

3.4. Shank3 knockdown inhibits D-gal-induced mitochondria-derived oxidative stress and mitochondria-dependent apoptosis

Cardiomyocyte apoptosis was detected by flow cytometry and Western blot analysis, with or without Shank3 knockdown. As shown in Fig. 4A–E, D-gal treatment remarkably induced cardiomyocytes apoptosis, as evidenced by elevated apoptotic cells, increased Bax levels, and decreased Bcl-2 levels. A loss in mitochondrial membrane potential (MMP) and an increase in mitochondrial-derived oxidative stress were observed, supporting the triggering of cardiomyocytes apoptosis. Therefore, we performed additional experiments to detect MMP and oxidative stress in the control and D-gal-treated cardiomyocytes. As shown in Fig. 4F and I, D-gal treatment induced a significant decline in

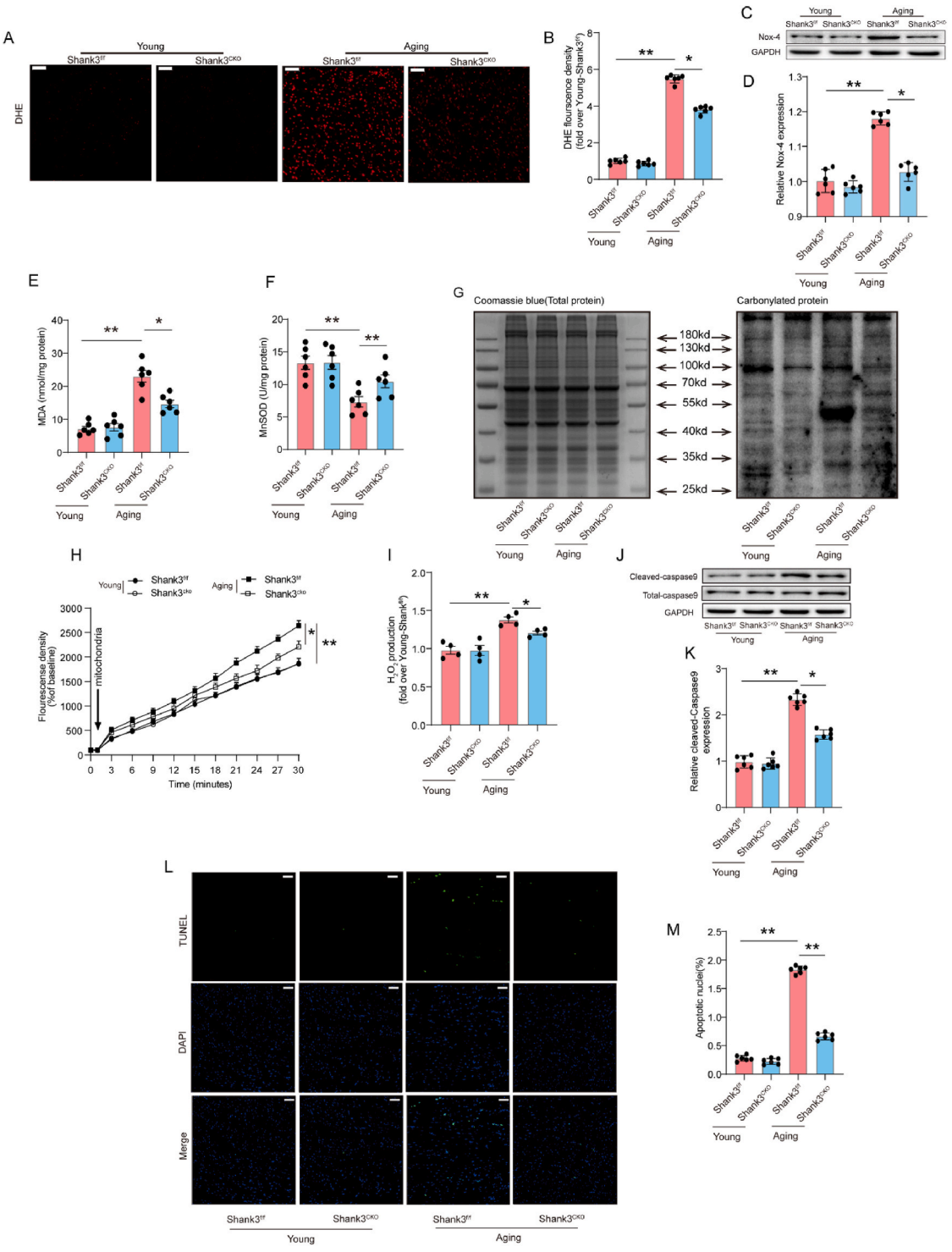

Fig. 2. Ablation of Shank3 inhibits mitochondria-derived superoxide production and cardiomyocyte apoptosis in senescence hearts. A Representative microphotograph of DHE staining in heart sections, Scale bar = 50 μm; **B** Quantitative analysis of DHE fluorescence density (fold change over young Shank3$^{f/f}$) (Mean ± SEM, n = 6 mice per group, *P<0.05, **P<0.01); **C&D** Representative blot images and quantitative analysis of Nox-4 expression (Mean ± SEM, n = 6 independent experiments, *P<0.05, **P<0.01); **E** Myocardial.
malondialdehyde (MDA) content (Mean ± SEM, n = 6 mice per group, *P<0.05, **P<0.01); **F** Mitochondrial manganese superoxide dismutase (MnSOD) activity (Mean ± SEM, n = 6 independent experiments, **P<0.01); **G** Carbonylated protein content of heart extracts were detected by Western-blot (right) combined with Coomassie blue staining (left). **H** Time-dependent rise of mitochondrial H_2O_2 related fluorescence density; **I** Isolated mitochondrial H_2O_2 production (Mean ± SEM, n = 4 independent experiments, *P<0.05, **P<0.01); **J** Representative blot images of cleaved-caspase 9; and **K** Quantitative analysis of cleaved-caspase 9 (Mean ± SEM, n = 6 independent experiments, *P<0.05, **P<0.01); **L** Representative photomicrographs of TUNEL-stained and DAPI-stained heart sections. Green fluorescence shows TUNEL-positive nuclei; Blue fluorescence shows nuclei of total cardiomyocytes (DAPI-positive), Scale bar = 50 μm; **M** Percentage of TUNEL-positive nuclei (Mean ± SEM, n = 6 mice per group, **P<0.01). (For interpretation of the references to colour in this figure legend, the reader is referred to the Web version of this article.)

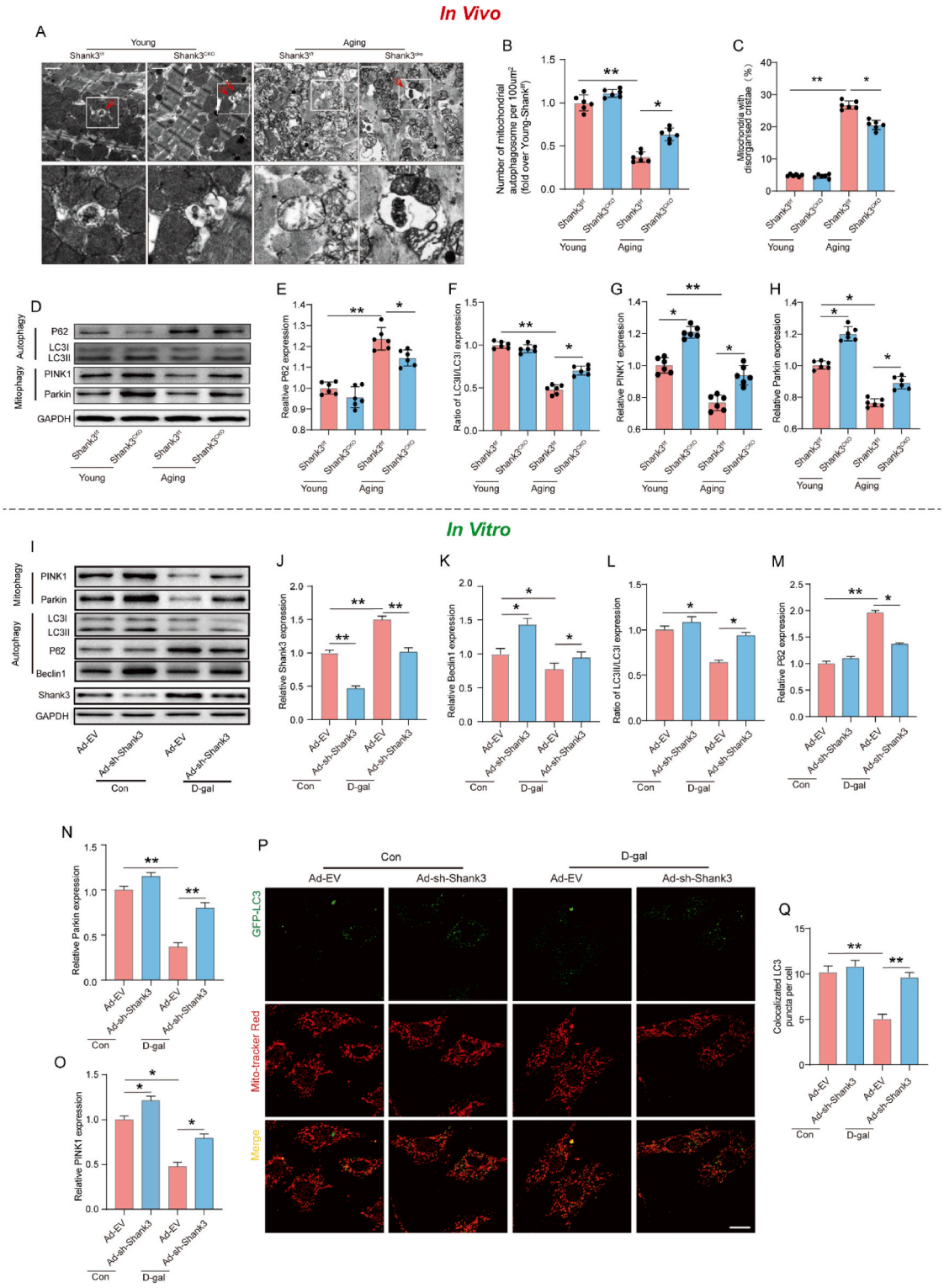

Fig. 3. Ablation of Shank3 restored mitophagy in aged hearts (*In Vivo*) and D-gal-treated cardiomyocytes (*In Vitro*). A, Ultrastructure of autophagosomes and mitochondria was observed using TEM. Scale bar = 2 μm; Red arrowheads denote autophagosomes encapsulating mitochondria. **B,** Number of mitochondrial autophagosomes per 100 μm^2. **C** Proportion of mitochondria with disorganized cristae were analyzed (Mean ± SEM, n = 6 images per group, *P<0.05, **P<0.01). **D** Representative blot images of autophagy proteins (LC3II/I and P62) and mitophagy proteins (PINK1, Parkin); **E&F** Quantitative analysis of LC3II/I and P62; **G&H** Quantitative analysis of PINK1 and Parkin. (Mean ± SEM, n = 6 independent experiments, *P<0.05, **P<0.01). **I–O** Representative gel blot images and quantitative analysis of Shank3 proteins, autophagy proteins (LC3II/I, P62 and Beclin1) and mitophagy proteins (PINK1, Parkin) using specific antibodies (Mean ± SEM, n = 6 independent experiments, *P<0.05, **P<0.01); **P** Representative confocal microscopic images showing mitophagy stained using Mito-Tracker Red and GFP-LC3, Scale bar = 20 μm; and **Q** Quantitative analysis of colocalized GFP-LC3 in primary cardiomyocytes.
(Mean ± SEM, n = 6 independent experiments, 30 cell were quantified per group, *P<0.05, **P<0.01). D-gal, D-galactosamine; Ad-sh-Shank3, adenovirus recombined with Shank3-shRNA. (For interpretation of the references to colour in this figure legend, the reader is referred to the Web version of this article.)

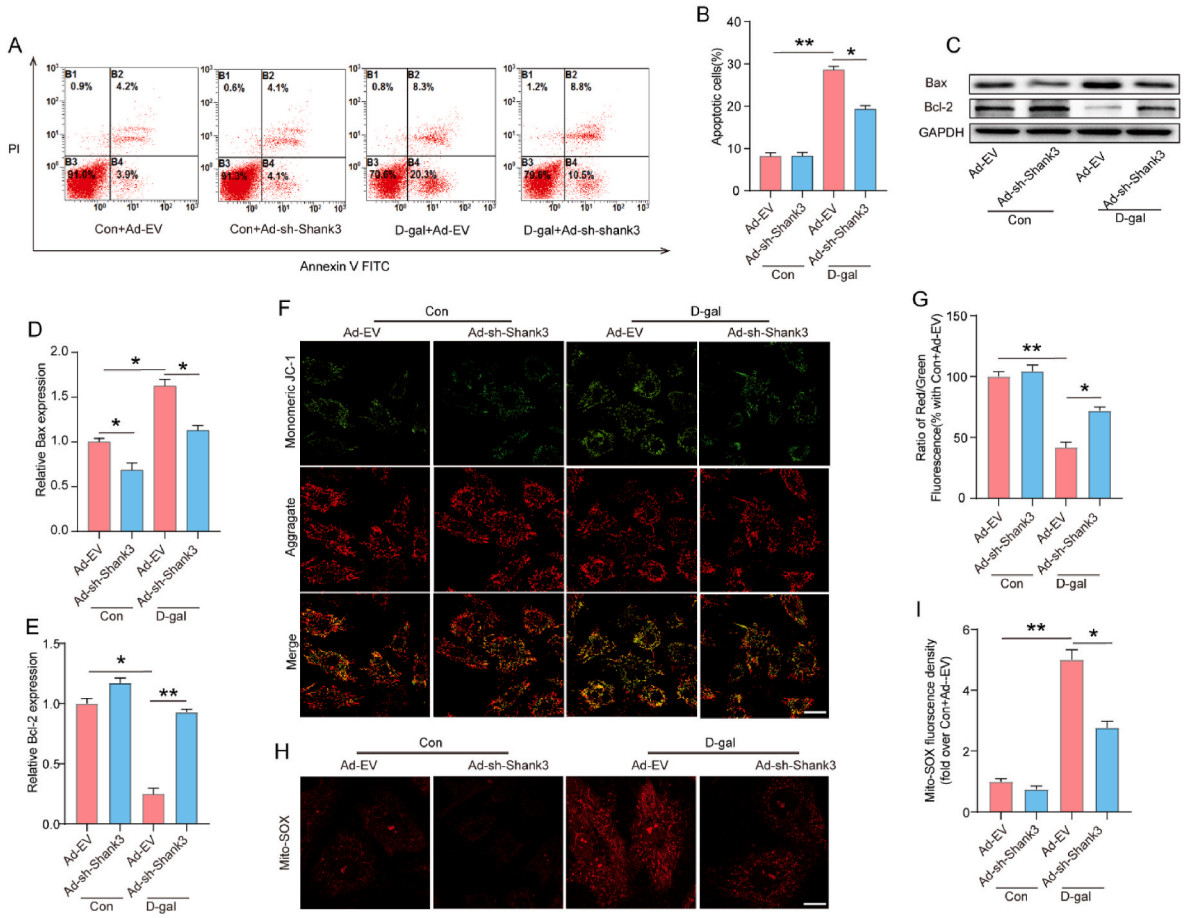

Fig. 4. Shank3 knockdown inhibited D-gal-induced mitochondria-derived oxidative stress and mitochondria-dependent apoptosis. **A** Flow cytometry analysis of apoptosis using annexin V and PI staining; **B** Quantification of apoptotic cells in primary cardiomyocytes (Mean ± SEM, n = 6 independent experiments, *P<0.05, **P<0.01); **C-E** Representative gel blot images and quantitative analysis of Bax and Bcl-2 (Mean ± SEM, n = 6 independent experiments, *P<0.05, **P<0.01); **F** Representative confocal microscopic images of JC-1 staining. Red fluorescence represents JC-1 aggregate and green fluorescence denotes JC-1 monomer. Scale bar = 20 μm; **G** Quantitative analysis of the ratio of aggregated and monomeric JC-1 (Mean ± SEM, n = 6 independent experiments, 30 cell were quantified per group, *P<0.05, **P<0.01); **H** Representative confocal microscopic images of Mito-SOX staining, Scale bar = 20 μm; and **I** Quantitative analysis of mitochondria-derived superoxide production in primary cardiomyocytes (Mean ± SEM, n = 6 independent experiments, 30 cell were quantified per group, *P<0.05, **P<0.01). D-gal, D-galactosamine; Ad-sh-Shank3, adenovirus recombined with Shank3-shRNA. (For interpretation of the references to colour in this figure legend, the reader is referred to the Web version of this article.)

MMP, while there was a significant increase in mitochondria-derived oxidative stress, as evidenced by the reduced ratio of aggregate/monomeric JC-1 and increased Mito-SOX fluorescence density. This suggests that D-gal-induced apoptosis is mitochondria-dependent. Consistent with our findings in mice hearts, knockdown of Shank3 significantly suppressed mitochondria-dependent cell apoptosis by elevating MMP, and reducing mitochondria-derived ROS production.

3.5. Shank3 overexpression mimicked D-gal-induced mitophagy inhibition, leading to mitochondria-derived oxidative stress and apoptosis in cardiomyocytes

To further reveal the effect of upregulated Shank3 on mitophagy and related myocardial injury, adenovirus recombined with Shank3 (Ad-Shank3) was employed to induce Shank3 overexpression in cardiomyocytes. In contrast to restored mitophagy activity in Shank3-knocked-down cells, Shank3 overexpression induced a significant mitophagy inhibition in normal treated cardiomyocytes, as well as suppressed autophagy activity, as indicated by changes in both mitophagy and autophagy indicators and reduced mitochondrial LC3 content (Fig. 5A–I). As a result, mitochondria-dependent cell apoptosis and mitochondria-derived superoxide anion production were also elevated by Shank3 overexpression, as indicated by an increased number of apoptotic cells, elevated Bax level, reduced Bcl-2 levels, decreased MMP levels, and increased Mito-SOX fluorescence density (Fig. 5J-R). MitoQ, a mitochondria-targeted antioxidant, was incubated with D-gal-treated or Shank3-overexpressed cardiomyocytes. As expected, MitoQ significantly ameliorated cell apoptosis induced by D-gal and Shank3 overexpression. These data suggested that Shank3-induced cardiomyocytes apoptosis is mitochondria-dependent (Fig. 6). In addition, mitochondrial biogenesis in normal cells was inhibited by Shank3 over-expression (Fig. 7). These data suggested that Shank3 overexpression induces D-gal-like mitophagy inhibition and myocardial injury in normal cultured cardiomyocytes, indicating the pivotal role of Shank3 in aging-related cardiac damage.

3.6. Enhanced Shank3-CaMKII binding and inhibition of parkin-mediated mitophagy in aged-hearts

Although upregulated Shank3 suppresses mitophagy in aging hearts, the underlying mechanisms remain unknown. Previous studies have reported that Shank3 physically interacts with CaMKII [40]. Another study demonstrated that CaMKII promotes the phosphorylation of Drp1, which is involved in mitochondrial fission [46]. Considering the close relationship between mitochondrial fission and mitophagy, we questioned whether Shank3 modulates mitophagy by binding to CaMKII in

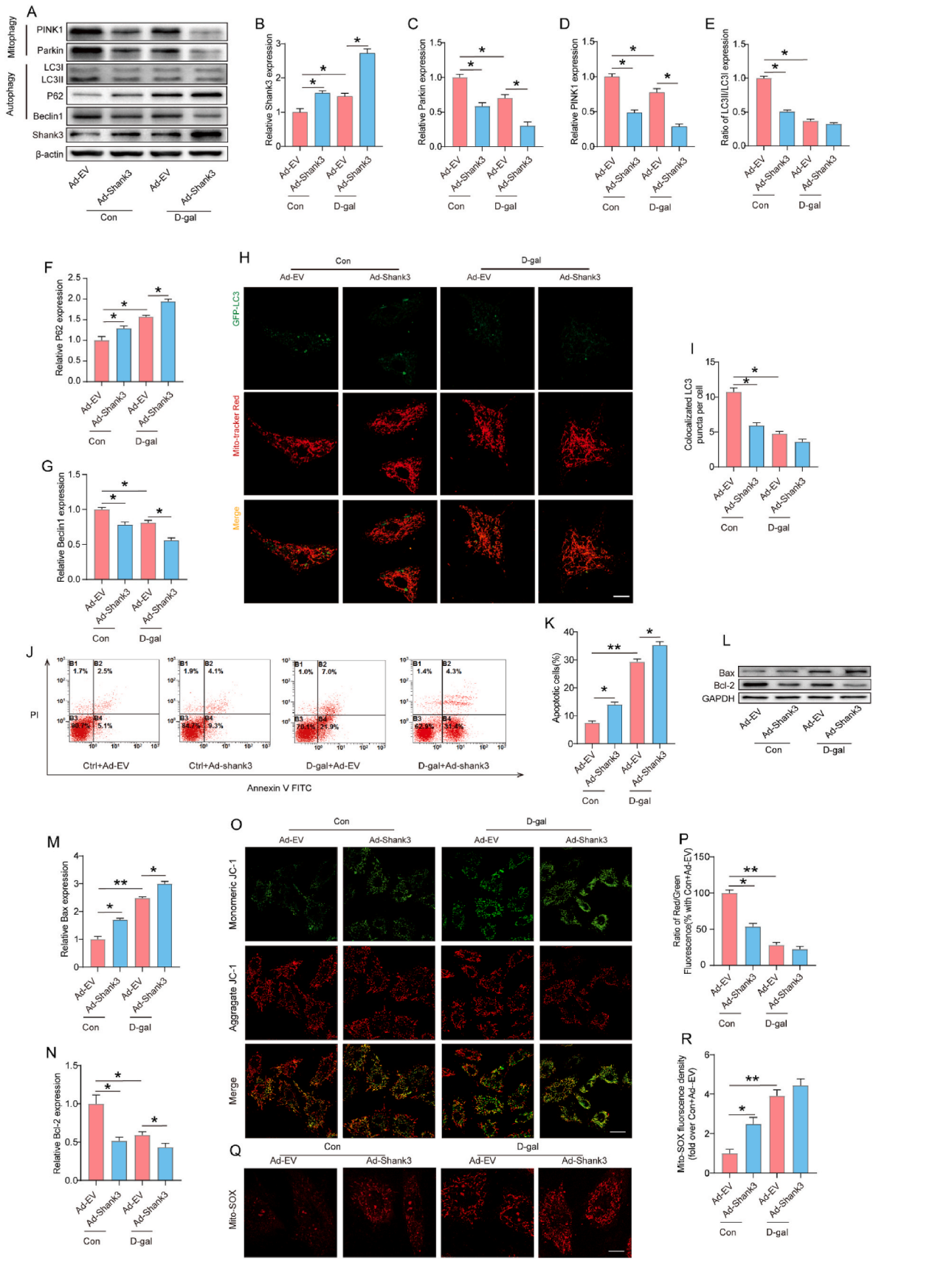

(caption on next page)

Fig. 5. Shank3 overexpression impeded mitophagy, leading to mitochondria-derived oxidative stress and apoptosis in cardiomyocytes. A-G Representative gel blot images and quantitative analysis of Shank3 proteins, autophagy proteins (LC3II/I, P62 and Beclin1) and mitophagy related proteins (PINK1, Parkin) (Mean ± SEM, n = 6 independent experiments, *P<0.05). **H** Representative confocal microscopic images showing mitophagy stained using Mito-Tracker Red and GFP-LC3, Scale bar = 20 μm; and **I** Quantitative analysis of colocalized GFP-LC3 in primary cardiomyocytes (Mean ± SEM, n = 6 independent experiments, 30 cell were quantified per group, *P<0.05, **P<0.01). **J** Flow cytometry analysis of apoptosis using annexin V and PI staining; **K** Quantification of apoptotic cells in primary cardiomyocytes (Mean ± SEM, n = 6 independent experiments, *P<0.05, **P<0.01); **L-N** Representative gel blot images and quantitative analysis of Bax and Bcl-2 (Mean ± SEM, n = 6 independent experiments, *P<0.05, **P<0.01); **O** Representative confocal microscopic images of JC-1 staining. Red fluorescence represents JC-1 aggregate and green fluorescence denotes JC-1 monomer. Scale bar = 20 μm; **P** Quantitative analysis of the ratio of aggregated and monomeric JC-1 (Mean ± SEM, n = 6 independent experiments, 30 cell were quantified per group, *P<0.05, **P<0.01); **Q** Representative confocal microscope images of Mito-SOX staining, Scale bar = 20 μm; and **R** Quantitative analysis of mitochondria derived superoxide production in primary cardiomyocytes (Mean ± SEM, n = 6 independent experiments, 30 cell were quantified per group, *P<0.05, **P<0.01). D-gal, D-galactosamine; Ad-Shank3, adenovirus recombined with Shank3. (For interpretation of the references to colour in this figure legend, the reader is referred to the Web version of this article.)

the aging heart. To test this hypothesis, a co-IP assay was conducted to detect the potential interactions between Shank3 and CaMKII in the heart (Fig. 6A and B). The co-IP results showed that Shank3 binds to CaMKII in cardiac tissue, and this binding is significantly enhanced in aged hearts (Fig. 6C and D). Immunofluorescence analysis further validated the interaction between Shank3 and CaMKII. Interestingly, D-gal treatment strengthened the co-localization of these two proteins and further altered the sub-cellular localization of CaMKII, with clumped CaMKII clustered at the periphery of the cell (Fig. 6E). The subcellular translocation of CaMKII from the cytoplasm to the mitochondria has been reported to modulate mitochondrial quality control. Thus, we performed an additional fluorescence analysis to detect the co-localization of CaMKII and mitochondria. As shown in Fig. 6F and G, D-gal treatment significantly reduced CaMKII-mitochondria co-localization, which was further validated by the reduced mitochondria-localized CaMKII detected by Western blot. Parkin translocation and phosphorylation are pivotal steps in mitophagy activation. As shown in Fig. 6H and I, in cardiomyocytes cultured in the control medium, Parkin was predominately positioned at the mitochondria, with few distributed in the cytoplasm. However, D-gal treatment impeded the mitochondrial translocation of Parkin and further decreased its phosphorylation level (Fig. 6H and I). These data suggest that Shank3-CaMKII binding is enhanced in aged hearts, which may be responsible for the reduced mitochondrial translocation of CaMKII and subsequent Parkin phosphorylation.

3.7. Shank3-induced inhibition of mitophagy was restored by CaMKII overexpression, whereas Shank3 ablation restored parkin-mediated mitophagy by promoting mitochondrial translocation of CaMKII in senescent cardiomyocytes

We investigated whether Shank3 ablation rescued D-gal-induced cardiomyocyte dysfunction in a PINK1/Parkin-dependent manner. PINK1 or Parkin was knocked down by siRNA transfection in senescent neonatal cardiomyocytes. As shown in Fig. 8, Shank3 ablation-induced mitophagy was significantly abolished by PINK1 or Parkin inhibition. Moreover, si-PINK or si-Parkin transfection blunted the protective effects of Shank3 ablation on cardiomyocytes function and mitochondrial function, as indicated by significantly increased Mito-SOX fluorescence density, decreased ratio of aggregate/monomeric JC-1 and higher apoptotic cell rate in si-PINK or si-Parkin transfected senescent cardiomyocytes. These data suggested that Shank3 ablation rescued senescence-induced mitophagy suppression and cardiomyocytes dysfunction in a PINK1/Parkin-dependent manner. Furthermore, to

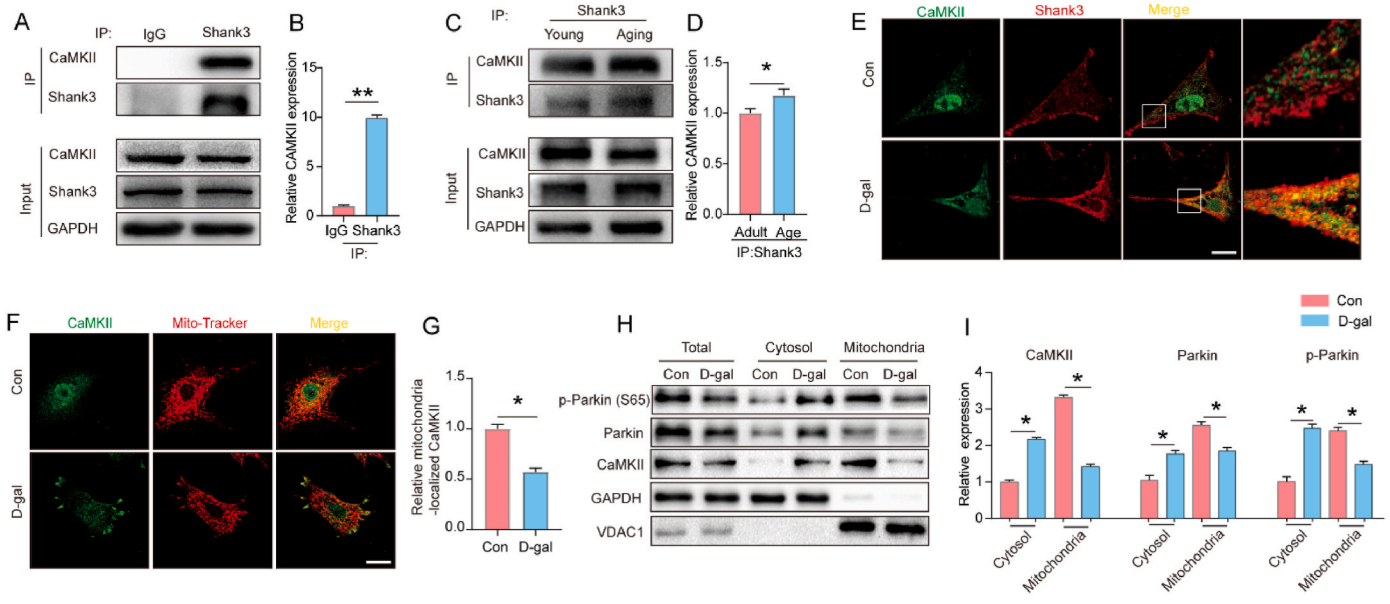

Fig. 6. Shank3 directly bond with CaMKII, which was associated with decreased mitochondrial translocation of CaMKII and parkin in the aged heart. A-B Interaction between Shank3 and CaMKII were detected by Co-IP (Mean ± SEM, n = 3 mice in each group, **P<0.01); **C-D** Interaction of Shank3 and CaMKII in hearts from young and aged mice were determined using Co-IP (Mean ± SEM, n = 3 mice in each group, **P<0.01); **E** Representative confocal microscopic images of Shank3 (Red) overlap with CaMKII (Green), Scale bar = 20 μm; **F** Representative confocal microscope images of CaMKII (Green) overlap with mitochondria (Red), Scale bar = 20 μm; **G** Mitochondria-localized CaMKII were analyzed using Pearson's coefficient analysis (Mean ± SEM, n = 6 independent experiments, 30 cell were quantified per group, *P<0.05); and **H&I** Representative gel blot images and quantitative analysis of CaMKII, Parkin and *p*-Parkin in total cardiomyocytes, cytosol and mitochondria (Mean ± SEM, n = 4 independent experiments, *P<0.05, **P<0.01). D-gal, D-galactosamine. (For interpretation of the references to colour in this figure legend, the reader is referred to the Web version of this article.)

discern the specific relationship between Shank3-CaMKII binding and Parkin-mediated mitophagy, the levels of Shank3 and CaMKII were modulated using an adenovirus. As shown in Fig. 7A, Shank3 overexpression evoked CaMKII distribution in a manner reminiscent of that in D-gal-challenged cells. Meanwhile, the translocation of CaMKII from the cytoplasm to the mitochondria was also impeded by Shank3 overexpression, as evidenced by decreased CaMKII-mitochondria co-localization (Fig. 7B and C). Mitochondrial translocation and phosphorylation of Parkin were further determined using mitochondrial isolation and Western blot. As shown in Fig. 7D-E, Shank3 overexpression lowered the protein level of Parkin and its phosphorylation in the mitochondria subcomponent in a manner reminiscent of D-gal. Interestingly, CaMKII overexpression remarkably restored CaMKII distribution, leading to a profound elevation in phosphorylated and mitochondria-localized Parkin. Similar to CaMKII overexpression, Shank3 ablation in D-gal-treated cells indued an obvious redistribution of CaMKII and Parkin from the cytosol to the mitochondria, leading to increased mitochondria-localized *p*-Parkin level (Fig. 7F–I). As a result, Shank3-induced inhibition of mitophagy in normal cultured cardiomyocytes was restored by CaMKII overexpression, whereas Shank3 ablation restored parkin-mediated mitophagy, as indicated by changes in mitochondria-localized LC3 puncta per cell (Fig. 7J and K). Taken together, these data suggest that upregulated Shank3 inhibits mitophagy in aged hearts in a CaMKII-dependent manner (see Fig. 8).

4. Discussion

In the present study, we identified Shank3 as a novel molecule involved in cardiac senescence and its underlying mechanism of action. First, we validated that elevated Shank3 expression and inhibited mitophagy in the aging heart results in mitochondrial dysfunction and excessive oxidative stress in aging hearts. Second, ablation of Shank3 restored mitophagy, alleviated mitochondrial dysfunction, suppressed mitochondria-derived oxidative stress, and consequently inhibited the development of aging-related cardiac dysfunction. Finally, we provided *in vivo* and *in vitro* evidence that Shank3 binds to CaMKII and impedes its translocation to the mitochondria, which further inhibits CaMKII activation and parkin-mediated mitophagy. Our study demonstrated for the first time that Shank3/CaMKII-induced mitophagy arrest is a pivotal contributor to age related cardiac dysfunction. Therefore, targeting mitophagy by regulating Shank3 may be a potential therapeutic strategy for cardiac senescence.

More than 90% of the ATP consumed for the normal contractile function of the heart is provided by the mitochondria. Mitochondria are primary organelles involved in oxidative stress and cell death signaling [47]. Mitochondrial hemostasis relies on the coordination of multiple quality control processes, including mitochondrial dynamics, mitophagy, and biogenesis [48]. Defective mitophagy has long been considered as a hallmark for senescent cardiomyocytes, leading to a general decline in mitochondrial function, accumulation of damaged mitochondria, and excessive ROS generation [49,50]. However, the reason for the mitophagy inhibition in aging hearts remains poorly defined. In this study, we observed that mitophagy is disturbed in aging hearts and senescent cardiomyocytes, accompanied by a significant upregulation of Shank3. Over-expression of Shank3 in cardiomyocytes evoked a senescence phenotype, manifested by inhibition of mitophagy. These results offer a novel mechanistic explanation for the age-dependent decline in mitochondrial integrity and the functional decline of the heart. In contrast, ablation of Shank3 in both the murine heart (*in vivo*) and cardiomyocytes (*in vitro*) restored mitophagy and improved cardiac function. Consistent with our results, numerous studies have revealed that the induction of mitophagy may be effective in preventing cardiac aging and other aging related organ dysfunction [51]. In addition to suppressed mitophagy, we also observed impaired mitochondrial biogenesis in senescent cardiomyocytes, indicating that the scarcity of new mitochondria may also be responsible for aging-associated functional decline in the heart. In lines with our results, a previous study suggested that mitophagy is closely coupled with mitochondrial biogenesis and that the damaged mitochondria degraded by mitophagy could be further used to generate new mitochondria [52]. To support this notion, the molecular signal involved in mitochondrial biogenesis was also activated by Shank3 knock-down, indicating that restoration of mitophagy in aging hearts would further promote mitochondrial biogenesis.

The PINK1/Parkin-mediated ubiquitin-dependent pathway plays a central role in mitophagy and maintains mitochondrial integrity and function [53,54]. Numerous studies have indicated that parkin is downregulated in various CVDs, including myocardial infarction, diabetic cardiomyopathy, and heart failure [55,56]. Notably, downregulation of Parkin was reported in the hearts of aged mice [57], whereas overexpression of Parkin alleviated functional decline in aged hearts [18]. Consistent with these results, we observed decreased levels of PINK1 and Parkin in the hearts of aging mice and senescent cardiomyocytes induced by D-gal. Moreover, data from our study also showed that the translocation of parkin from the cytoplasm to the mitochondria decreased in the aging heart, accompanied by a decreased in its phosphorylation. In the initial stage of the PINK1/Parkin-mediated ubiquitin-dependent pathway, loss of mitochondrial membrane potential leads to buildup of PINK1 on the outer mitochondrial membrane, where PINK1 in turn recruits Parkin from the cytoplasm to the mitochondria, prior to parkin phosphorylation [58]. Therefore, the translocation and subsequent phosphorylation of parkin is a critical step in mitophagy induction. In addition to up-regulating PINK1 and Parkin expression, Shank3 knockdown in senescent cardiomyocytes promoted the mitochondrial translocation of Parkin as well as its phosphorylation, leading to the restoration of mitophagy and mitochondrial function. In contrast, Shank3 inhibition in normal cardiomyocytes significantly impeded the translocation and phosphorylation of parkin. Consistently, a previous study reported that elevated mitochondrial Parkin translocation promoted mitophagy in the hearts of aging mice, and consequently retarded cardiac aging [59]. However, another independent study demonstrated a concurrent accumulation of parkin in the aged heart and cardiac-specific parkin overexpression led to increased perivascular fibrosis in aged hearts [60]. These findings suggested that Parkin-mediated mitophagy should be adjusted to an appropriate degree to maintain the efficient clearance of damaged mitochondria in aged hearts and that both excessively strong and weak mitophagy would cause the disrupts mitochondrial homeostasis and further cardiac injury.

As the best-examined member of the Shank family, Shank3 was initially reported to participate in the pathogenesis of neurological disorders including autism spectrum disorder and age-related neurodegeneration [22]. Although studies have revealed the enrichment of Shank3 in cardiac tissues, its role Shank3 in the physiological and pathophysiological processes of the heart remains elusive [28]. To the best of our knowledge, little evidence is available regarding the role of Shank3 in cardiac aging. In this study, we demonstrated for the first time that upregulated Shank3 is a pivotal contributor to the pathogenesis of age-related cardiac anomalies. In contrast, Shank3 ablation in murine hearts protected against age-induced cardiomyopathy by restoring mitophagy, leading to preserved mitochondrial integrity and reduced mitochondria-derived oxidative stress. In addition to defective mitophagy, previous studies have reported a loss of autophagy throughout the course of aging, contributing to compromised cardiac function [50]. Interestingly, in this study, we found that the inhibition of autophagy in aging hearts and senescent cardiomyocytes was restored by Shank3 ablation. This result supports that Shank3 may functions as an autophagy regulator. However, recent findings from a myocardial infarction setting revealed that Shank3 overexpression evoked autophagy to suppress apoptosis [61]. This discrepancy might be due to the different mouse models employed in these studies (full-body Shank3 overexpression *vs.* cardiac-specific Shank3 knockout), suggesting that changes in global Shank3 would also cause altered autophagy activity in

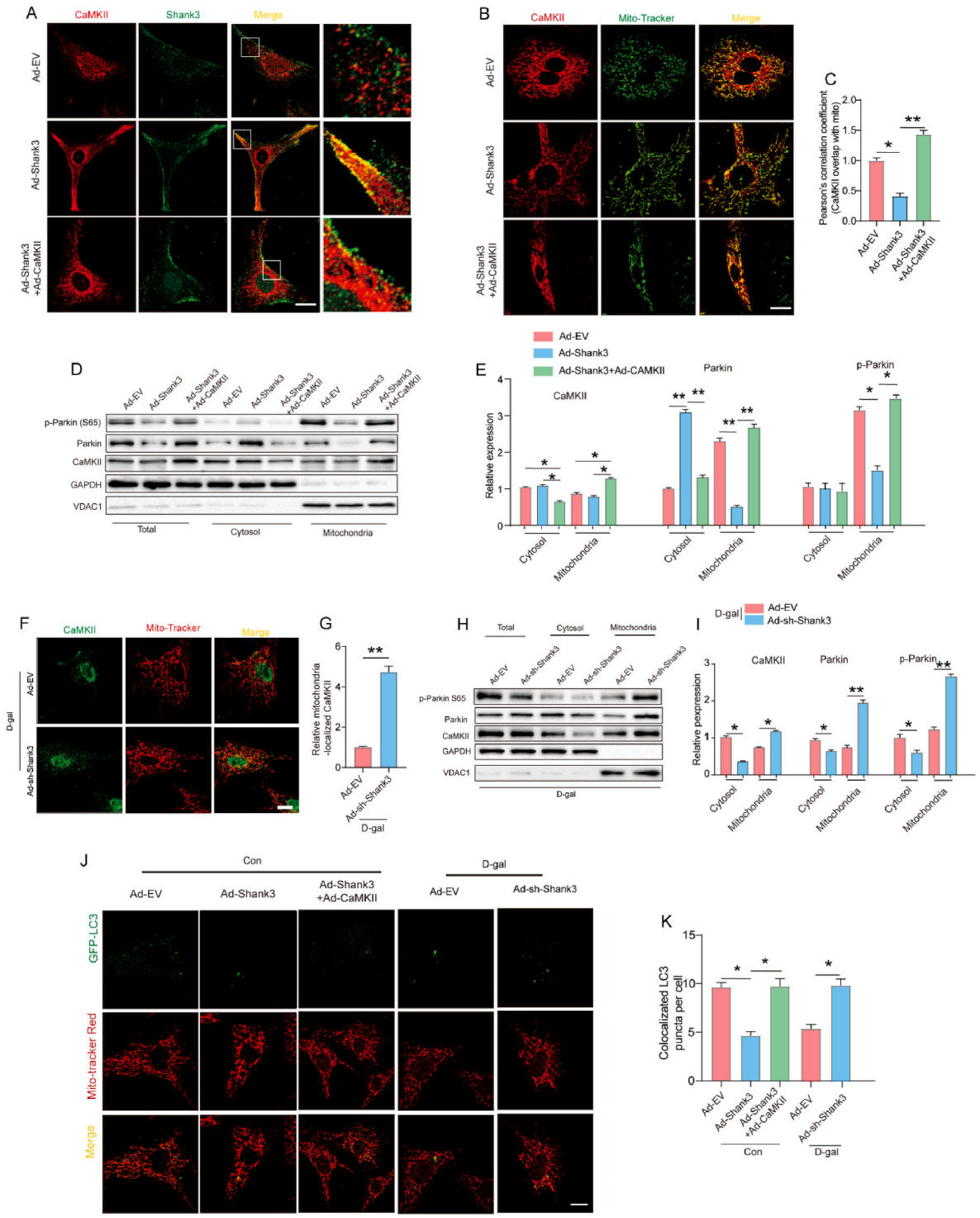

Fig. 7. Shank3-induced inhibition of mitophagy were restored by CaMKII overexpression, while Shank3 ablation restored parkin-mediated mitophagy by promoting mitochondrial translocation of CaMKII in senescent cardiomyocytes. A Representative confocal microscopic images of Shank3 overlap with CaMKII, Scale bar = 20 μm; **B** Representative confocal microscopic images of CaMKII overlap with mitochondria, Scale bar = 20 μm; **C** Relative cellular localization of CaMKII and mitochondria quantified using Pearson's coefficient analysis (Mean ± SEM, n = 6 independent experiments, 30 cell were quantified per group, *P<0.05, **P<0.01); **D&E** Representative gel blot images and quantitative analysis of CaMKII, Parkin and *p*-Parkin in total cardiomyocytes, cytosol and mitochondria (Mean ± SEM, n = 4 independent experiments, *P<0.05, **P<0.01); **F&G** Representative confocal microscope images of CaMKII overlap with mitochondria, and Mitochondria-localized CaMKII was quantified by Pearson's coefficient analysis, Scale bar = 20 μm (n = 6 independent experiments each group); **H&I** Representative blot images and quantitative analysis of CaMKII, Parkin and *p*-Parkin separately in total cardiomyocytes, cytosol and mitochondria (Mean ± SEM, n = 4 independent experiments, *P<0.05, **P<0.01); **J** Representative confocal microscope images showing mitophagy stained by Mito-tracker and GFP-LC3, Scale bar = 20 μm. **K** Quantitative analysis of mitochondria-localized GFP-LC3 in primary cardiomyocytes. (Mean ± SEM, n = 6 independent experiments, 30 cell were quantified per group, *P<0.05, **P<0.01). D-gal, D-galactosamine; Ad-Shank3, adenovirus recombined with Shank3. Ad-sh-Shank3, adenovirus recombined with Shank3-shRNA, Ad-CaMKII, adenovirus recombined with CaMKII.

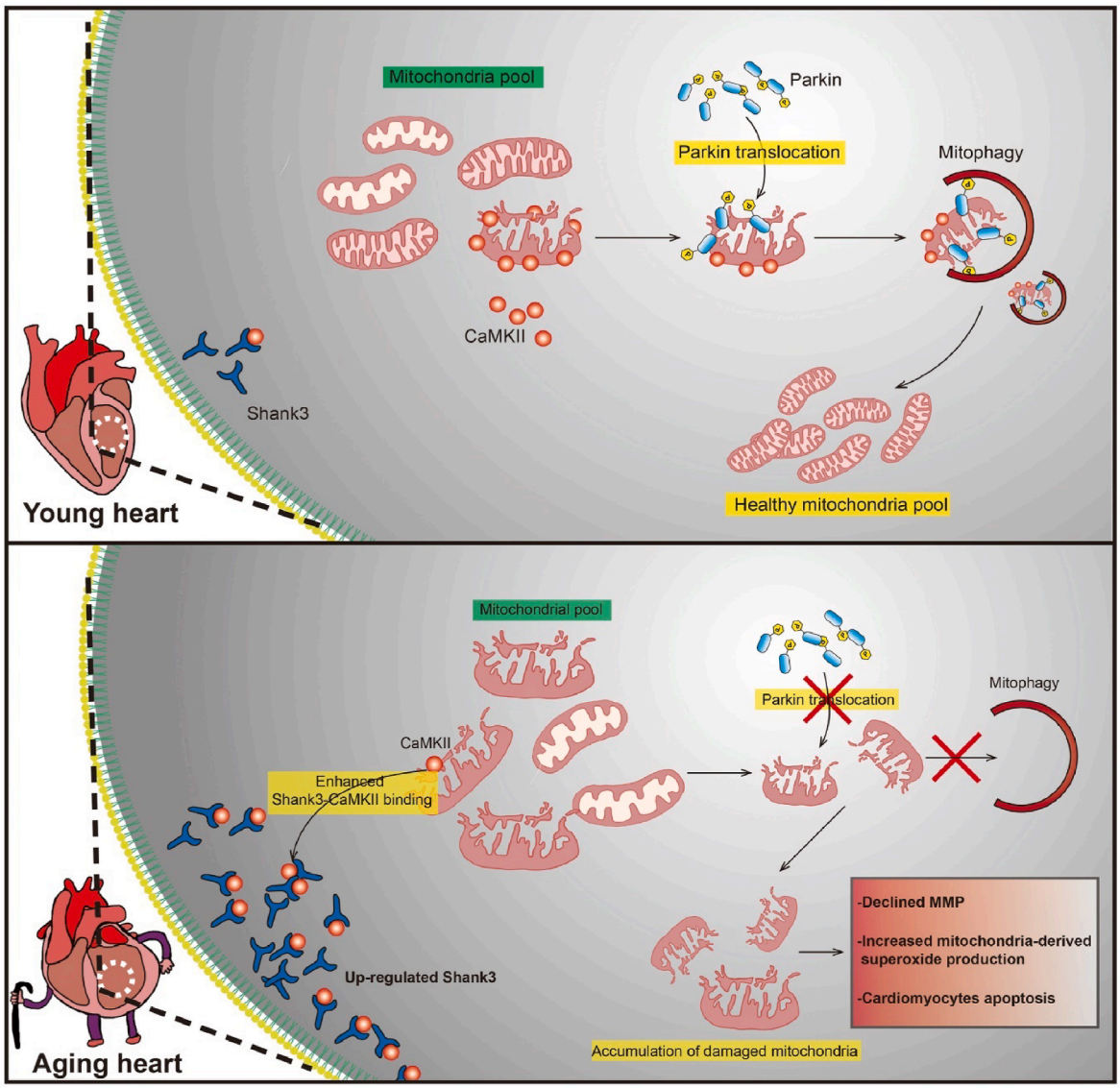

Fig. 8. Schematic diagram illustrating that elevated Shank3 binds with CaMKII and impedes its mitochondrial translocation, resulting in inhibition of parkin-mediated mitophagy, which ultimately leads to mitochondrial dysfunction and cardiac damage in the aged heart.
Under cardiac aging, upregulated Shank3 binds with CaMKII to impede its mitochondrial translocation, suppressing mitochondrial translocation of Parkin and Parkin-mediated mitophagy. Mitophagy inhibition induced by Shank3/CaMKII binding evokes collapse of mitochondrial membrane potential, promotes mitochondria-derived superoxide production and mitochondria-dependent cardiomyocyte apoptosis, leading to aging-related cardiac dysfunction.

the heart. Considering the critical role of disrupted mitophagy and autophagy in multiple CVDs, further studies are needed to reveal the role of Shank3 in CVDs other than cardiac aging.

Another intriguing finding from the present study is that Shank3-induced mitophagy loss relies on the binding with CaMKII, which impedes the translocation of CaMKII from the cytoplasm to the mitochondria. The following scenario can be considered. First, Shank3 physically interacts with CaMKII, and this interaction is stronger in aged hearts than in adult hearts. Second, Shank3 overexpression decreased the co-localization of CaMKII and mitochondria, leading to reduced phosphorylation of Parkin, and mitochondria-localized Parkin. Finally, CaMKII overexpression restored CaMKII distribution and further reversed mitophagy arrest in Shank3-overexpressed cardiomyocytes. Taken together, these results support the key role of Shank3-CamKII binding in mitophagy and mitochondrial quality control in aging hearts. CaMKII is a multi-functional protein kinase that controls the transmission of calcium signaling to regulate various cellular process [62,63]. Recent evidence has demonstrated that CaMKII activation promotes mitochondrial fission by regulating Drp1 phosphorylation at S616. Further studies also revealed that mitochondrial translocation of CaMKII contributes to mitochondrial translocation and phosphorylation of Drp1 [46]. Similar to these findings, the results from our current study suggest that activation of CaMKII in aged hearts promotes mitophagy by regulating mitochondrial translocation and phosphorylation of Parkin. To the best of our knowledge, this is the first report to show that mitochondrial translocation of CaMKII induces mitochondrial translocation and phosphorylation of Parkin, promoting mitophagy. The concerted interplay between mitochondrial fission and mitophagy has been well conceived in numerous studies [64,65], where damaged mitochondria are segregated from the healthy mitochondrial pool and are further degraded by mitophagy [52]. Since activation of Drp1 and Parkin is regulated by CaMKII translocation, CaMKII may function as a central regulator of mitochondrial quality control processes. CaMKII is believed to be responsible for the phosphorylation of multiple molecules owing to its kinase activity [66]. However, the exact mechanisms by which CaMKII promotes Parkin phosphorylation are still unknown. We failed

to detect a direct interaction between CaMKII and Parkin, indicating that CaMKII indirectly promoted Parkin translocation (data not shown). Interestingly, it has been reported that CaMKII promotes mPTP opening by increasing Drp1 activation and mitochondrial calcium uniporter current, thereby decreasing the MMP [46,67]. Consequently, decreased MMP leads to the phosphorylation and recruitment of Parkin to the mitochondria. Although the complex of Shank3 and CaMKII has been reported in synapse of neuronal cells [40], previous studies have used Shank3 as a substrate for CaMKII, for which CaMKII was confirmed to regulate the phosphorylation and synaptic enrichment of Shank3. In this study, we uniquely proposed that Shank3-CaMKII binding can, in turn, change the sub-cellular distribution of CaMKII by impeding its translocation to the mitochondria. These results improve the current knowledge on the modulation ways of CaMKII activity, especially in the cardiovascular system.

Our study has several limitations. First, our *in vivo* experiments were conducted on cardiac-specific Shank3 knockout mice, a "gain-of-function" cardiac-specific Shank3 transgenic mice would provide a more intuitive role of Shank3 in the regulation of cardiac homeostasis. Second, considering the pivotal role of mitochondria and CaMKII in cellular Ca^{2+} transport [68], Ca^{2+} homeostasis.

in the mitochondria might also be influenced by Shank3 ablation/overexpression. Further studies are needed to explore the impact of Shank3 on cellular Ca^{2+} signaling. Despite these limitations, this study offers novel insights into the pathogenesis of aging-related cardiac dysfunction and the regulatory mechanism of mitophagy in the hearts.

In summary, our study demonstrated for the first time that upregulated Shank3 levels arre likely responsible for reduced mitophagy and mitochondrial homeostasis in aging hearts. Ablation of Shank3 restored mitophagy by activating the mitochondrial translocation of CaMKII/Parkin, leading to improved mitochondrial function, decreased mitochondrial-derived oxidative stress, and consequently preserved cardiac function during aging. These results revealed that Shank3-modulated mitophagy is a promising and feasible therapeutic target for the clinical management of aging-related cardiac dysfunction.

Authors' contribution

M.Z. and Y.L. conceived and designed the study. Y.W., Y.F., L.H., R. W. and R.Z. performed the animal experiments. Y.W., Y.X., W.G., L.H., D.G., B.Q. and G.R. carried out the cell experiments. Y.W., Y.X., W.G. and Y.F. analyzed the data. Y.W. drafted the manuscript. M.Z., J.R. and Y.L. revised and edited the manuscript. All authors have read and approved the final version of this manuscript.

Funding information

This work was supported by the National Natural Science Foundation of China (No.81900338 & No.82270366) and Shaanxi Province Science and Technology New Star Project (2022KJXX-107).

Acknowledgements

We appreciate Dr. Zhelong Li from Department of Ultrasound Diagnostics, Tangdu Hospital for his excellent technical assistance.

Abbreviations

ATP	adenosine-triphosphate
Bax	Bcl-2 associated X protein
Bcl-2	B-celllymphoma-2
CaMKII	Ca2+/calmodulin-dependent protein kinase II
Co-IP	Co-immunoprecipitation
CVDs	Cardiovascular diseases
D-gal	D-galactosamine
DHE	Dihydroethidium
Drp1	dynamic-related protein1
H_2O_2	Hydrogen peroxide
LC3	Microtuble-associated protein 1 light chain 3
LVEF	left ventricular ejection fraction
LVFS	left ventricular fraction shortening
MMP	mitochondrial membrane potential
Nox4	NADPH oxidase 4
NRF-1	Nuclar respiratory factor-1
Parkin	parkin RBR E3 ubiquitin-protein ligase
Pink1	PTEN induced putative kinase 1
PGC-1α	Peroxisome proliferator-activated receptor gamma co-activator 1-alpha
P62	Sequestosome 1, SQSTM1
ROS	reactive oxygen spices
SA β-Gal	senescence-associated β-galactosidase
Shank3	SH3 and multiple ankyrin repeat domains protein 3
TEM	Transmission electronic microscopy
TFAM	Mitochondrial transcription factor A
TUNEL	Terminal-deoxynucleotidyl transferase mediated nick end labeling
VDAC1	Voltage-dependent anion channel 1
WGA	Wheat Germ Agglutinin

Appendix A. Supplementary data

Supplementary data to this article can be found online at https://doi.org/10.1016/j.redox.2022.102537.

References

[1] E.J. Benjamin, M.J. Blaha, S.E. Chiuve, M. Cushman, S.R. Das, R. Deo, S.D. de Ferranti, J. Floyd, M. Fornage, C. Gillespie, C.R. Isasi, M.C. Jimenez, L.C. Jordan, S. E. Judd, D. Lackland, J.H. Lichtman, L. Lisabeth, S. Liu, C.T. Longenecker, R. H. Mackey, K. Matsushita, D. Mozaffarian, M.E. Mussolino, K. Nasir, R.W. Neumar, L. Palaniappan, D.K. Pandey, R.R. Thiagarajan, M.J. Reeves, M. Ritchey, C. J. Rodriguez, G.A. Roth, W.D. Rosamond, C. Sasson, A. Towfighi, C.W. Tsao, M. B. Turner, S.S. Virani, J.H. Voeks, J.Z. Willey, J.T. Wilkins, J.H. Wu, H.M. Alger, S. S. Wong, P. Muntner, C. American Heart Association Statistics, S. Stroke Statistics, Heart disease and stroke statistics-2017 update: a report from the American heart association, Circulation 135 (10) (2017) e146–e603.

[2] S. Nanayakkara, T.H. Marwick, D.M. Kaye, The ageing heart: the systemic and coronary circulation, Heart 104 (5) (2018) 370–376.

[3] M.S. Denzel, N.J. Storm, A. Gutschmidt, R. Baddi, Y. Hinze, E. Jarosch, T. Sommer, T. Hoppe, A. Antebi, Hexosamine pathway metabolites enhance protein quality control and prolong life, Cell 156 (6) (2014) 1167–1178.

[4] T. Finkel, M. Serrano, M.A. Blasco, The common biology of cancer and ageing, Nature 448 (7155) (2007) 767–774.

[5] M.B. Jensen, H. Jasper, Mitochondrial proteostasis in the control of aging and longevity, Cell Metabol. 20 (2) (2014) 214–225.

[6] T.E.S. Kauppila, J.H.K. Kauppila, N.G. Larsson, Mammalian mitochondria and aging: an update, Cell Metabol. 25 (1) (2017) 57–71.

[7] Y. Wang, Y. Li, C. He, B. Gou, M. Song, Mitochondrial regulation of cardiac aging, Biochim. Biophys. Acta, Mol. Basis Dis. 1865 (7) (2019) 1853–1864.

[8] E.A. Abdel-Rahman, S. Hosseiny, A. Aaliya, M. Adel, B. Yasseen, A. Al-Okda, Y. Radwan, S.H. Saber, N. Elkholy, E. Elhanafy, E.E. Walker, J.P. Zuniga-Hertz, H. H. Patel, H.R. Griffiths, S.S. Ali, Sleep/wake calcium dynamics, respiratory function, and ROS production in cardiac mitochondria, J. Adv. Res. 31 (2021) 35–47.

[9] K.C. Das, H. Muniyappa, Age-dependent mitochondrial energy dynamics in the mice heart: role of superoxide dismutase-2, Exp. Gerontol. 48 (9) (2013) 947–959.

[10] O. Bergmann, R.D. Bhardwaj, S. Bernard, S. Zdunek, F. Barnabé-Heider, S. Walsh, J. Zupicich, K. Alkass, B.A. Buchholz, H. Druid, S. Jovinge, J. Frisén, Evidence for cardiomyocyte renewal in humans, Science 324 (5923) (2009) 98–102.

[11] R.J. Youle, D.P. Narendra, Mechanisms of mitophagy, Nat. Rev. Mol. Cell Biol. 12 (1) (2011) 9–14.

[12] H. Enomoto, N. Mittal, T. Inomata, T. Arimura, T. Izumi, A. Kimura, K. Fukuda, S. Makino, Dilated cardiomyopathy-linked heat shock protein family D member 1 mutations cause up-regulation of reactive oxygen species and autophagy through mitochondrial dysfunction, Cardiovasc. Res. 117 (4) (2021) 1118–1131.

[13] M. Tong, T. Saito, P. Zhai, S.I. Oka, W. Mizushima, M. Nakamura, S. Ikeda, A. Shirakabe, J. Sadoshima, Alternative mitophagy protects the heart against obesity-associated cardiomyopathy, Circ. Res. 129 (12) (2021) 1105–1121.

[14] M. Babbar, S. Basu, B. Yang, D.L. Croteau, V.A. Bohr, Mitophagy and DNA damage signaling in human aging, Mech. Ageing Dev. 186 (2020), 111207.

[15] D.P.W. Jayatunga, E. Hone, P. Bharadwaj, M. Garg, G. Verdile, G.J. Guillemin, R. N. Martins, Targeting mitophagy in Alzheimer's disease, J Alzheimers Dis 78 (4) (2020) 1273–1297.

[16] X. Liu, C. Yang, Y. Deng, P. Liu, H. Yang, X. Du, Y. Du, Polygoni multiflori radix preparat delays skin aging by inducing mitophagy, BioMed Res. Int. 2021 (2021), 5847153.
[17] E.F. Fang, Y. Hou, K. Palikaras, B.A. Adriaanse, J.S. Kerr, B. Yang, S. Lautrup, M. M. Hasan-Olive, D. Caponio, X. Dan, P. Rocktaschel, D.L. Croteau, M. Akbari, N. H. Greig, T. Fladby, H. Nilsen, M.Z. Cader, M.P. Mattson, N. Tavernarakis, V. A. Bohr, Mitophagy inhibits amyloid-beta and tau pathology and reverses cognitive deficits in models of Alzheimer's disease, Nat. Neurosci. 22 (3) (2019) 401–412.
[18] A. Hoshino, Y. Mita, Y. Okawa, M. Ariyoshi, E. Iwai-Kanai, T. Ueyama, K. Ikeda, T. Ogata, S. Matoba, Cytosolic p53 inhibits Parkin-mediated mitophagy and promotes mitochondrial dysfunction in the mouse heart, Nat. Commun. 4 (2013) 2308.
[19] A. Rana, M. Rera, D.W. Walker, Parkin overexpression during aging reduces proteotoxicity, alters mitochondrial dynamics, and extends lifespan, Proc. Natl. Acad. Sci. U. S. A. 110 (21) (2013) 8638–8643.
[20] D. Ryu, L. Mouchiroud, P.A. Andreux, E. Katsyuba, N. Moullan, A.A. Nicolet-Dit-Felix, E.G. Williams, P. Jha, G. Lo Sasso, D. Huzard, P. Aebischer, C. Sandi, C. Rinsch, J. Auwerx, Urolithin A induces mitophagy and prolongs lifespan in C. elegans and increases muscle function in rodents, Nat. Med. 22 (8) (2016) 879–888.
[21] S. Naisbitt, E. Kim, J.C. Tu, B. Xiao, C. Sala, J. Valtschanoff, R.J. Weinberg, P. F. Worley, M. Sheng, Shank, a novel family of postsynaptic density proteins that binds to the NMDA receptor/PSD-95/GKAP complex and cortactin, Neuron 23 (3) (1999) 569–582.
[22] P. Monteiro, G. Feng, SHANK proteins: roles at the synapse and in autism spectrum disorder, Nat. Rev. Neurosci. 18 (3) (2017) 147–157.
[23] S. Uchino, C. Waga, Novel therapeutic approach for autism spectrum disorder: focus on SHANK3, Curr. Neuropharmacol. 13 (6) (2015) 786–792.
[24] H.J. Kreienkamp, Scaffolding proteins at the postsynaptic density: shank as the architectural framework, Handb. Exp. Pharmacol. 186 (2008) 365–380.
[25] E. Marcello, M. Di Luca, F. Gardoni, Synapse-to-nucleus communication: from developmental disorders to Alzheimer's disease, Curr. Opin. Neurobiol. 48 (2018) 160–166.
[26] C. Grasselli, A. Carbone, P. Panelli, V. Giambra, M. Bossi, G. Mazzoccoli, L. De Filippis, Neural stem cells from shank3-ko mouse model autism spectrum disorders, Mol. Neurobiol. 57 (3) (2020) 1502–1515.
[27] N. Mizban, N. Vousooghi, N. Mizban, Association of SHANK3 gene polymorphism and Parkinson disease in the north of Iran, Basic Clin. Neurosci. 12 (1) (2021) 57–62.
[28] D.R. Grubb, P. Iliades, N. Cooley, Y.L. Yu, J. Luo, T.M. Filtz, E.A. Woodcock, Phospholipase Cbeta1b associates with a Shank3 complex at the cardiac sarcolemma, Faseb. J. 25 (3) (2011) 1040–1047.
[29] H. Ji, A.C. Kwan, M.T. Chen, D. Ouyang, J.E. Ebinger, S.P. Bell, T.J. Niiranen, N. A. Bello, S. Cheng, Sex differences in myocardial and vascular aging, Circ. Res. 130 (4) (2022) 566–577.
[30] H. Bartolomaeus, A. Balogh, M. Yakoub, S. Homann, L. Markó, S. Höges, D. Tsvetkov, A. Krannich, S. Wundersitz, E.G. Avery, N. Haase, K. Kräker, L. Hering, M. Maase, K. Kusche-Vihrog, M. Grandoch, J. Fielitz, S. Kempa, M. Gollasch, Z. Zhumadilov, S. Kozhakhmetov, A. Kushugulova, K.U. Eckardt, R. Dechend, L.C. Rump, S.K. Forslund, D.N. Müller, J. Stegbauer, N. Wilck, Short-chain fatty acid propionate protects from hypertensive cardiovascular damage, Circulation 139 (11) (2019) 1407–1421.
[31] C.C. Hsieh, C.Y. Li, C.H. Hsu, H.L. Chen, Y.H. Chen, Y.P. Liu, Y.R. Liu, H.F. Kuo, P. L. Liu, Mitochondrial protection by simvastatin against angiotensin II-mediated heart failure, Br. J. Pharmacol. 176 (19) (2019) 3791–3804.
[32] L.P. Zhu, T. Tian, J.Y. Wang, J.N. He, T. Chen, M. Pan, L. Xu, H.X. Zhang, X.T. Qiu, C.C. Li, K.K. Wang, H. Shen, G.G. Zhang, Y.P. Bai, Hypoxia-elicited mesenchymal stem cell-derived exosomes facilitates cardiac repair through miR-125b-mediated prevention of cell death in myocardial infarction, Theranostics 8 (22) (2018) 6163–6177.
[33] C. Hu, X. Zhang, W. Wei, N. Zhang, H. Wu, Z. Ma, L. Li, W. Deng, Q. Tang, Matrine attenuates oxidative stress and cardiomyocyte apoptosis in doxorubicin-induced cardiotoxicity via maintaining AMPKα/UCP2 pathway, Acta Pharm. Sin. B 9 (4) (2019) 690–701.
[34] B. Bostick, A.R. Aroor, J. Habibi, W. Durante, L. Ma, V.G. DeMarco, M. Garro, M. R. Hayden, F.W. Booth, J.R. Sowers, Daily exercise prevents diastolic dysfunction and oxidative stress in a female mouse model of western diet induced obesity by maintaining cardiac heme oxygenase-1 levels, Metabolism 66 (2017) 14–22.
[35] Y. Hong, H. He, G. Jiang, H. Zhang, W. Tao, Y. Ding, D. Yuan, J. Liu, H. Fan, F. Lin, X. Liang, X. Li, Y. Zhang, miR-155-5p inhibition rejuvenates aged mesenchymal stem cells and enhances cardioprotection following infarction, Aging Cell 19 (4) (2020), e13128.
[36] J. Jin, S. Qiu, P. Wang, X. Liang, F. Huang, H. Wu, B. Zhang, W. Zhang, X. Tian, R. Xu, H. Shi, X. Wu, Cardamonin inhibits breast cancer growth by repressing HIF-1α-dependent metabolic reprogramming, J. Exp. Clin. Cancer Res. 38 (1) (2019) 377.
[37] E.T. Chouchani, V.R. Pell, A.M. James, L.M. Work, K. Saeb-Parsy, C. Frezza, T. Krieg, M.P. Murphy, A unifying mechanism for mitochondrial superoxide production during ischemia-reperfusion injury, Cell Metabol. 23 (2) (2016) 254–263.
[38] J. Geng, D.J. Klionsky, Direct quantification of autophagic flux by a single molecule-based probe, Autophagy 13 (4) (2017) 639–641.
[39] X. Bian, D. Shi, K. Xing, H. Zhou, L. Lu, D. Yu, W. Wu, AMD1 upregulates hepatocellular carcinoma cells stemness by FTO mediated mRNA demethylation, Clin. Transl. Med. 11 (3) (2021) e352.
[40] T.L. Perfitt, X. Wang, M.T. Dickerson, J.R. Stephenson, T. Nakagawa, D. A. Jacobson, R.J. Colbran, Neuronal L-type calcium channel signaling to the nucleus requires a novel CaMKIIα-shank3 interaction, J. Neurosci. 40 (10) (2020) 2000–2014.
[41] W. Stauffer, H. Sheng, H.N. Lim, EzColocalization: an ImageJ plugin for visualizing and measuring colocalization in cells and organisms, Sci. Rep. 8 (1) (2018), 15764.
[42] Y. Zhang, I. Naguro, A.E. Herr, In situ single-cell western blot on adherent cell culture, Angew Chem. Int. Ed. Engl. 58 (39) (2019) 13929–13934.
[43] Y. He, L. Zhou, Z. Fan, S. Liu, W. Fang, Palmitic acid, but not high-glucose, induced myocardial apoptosis is alleviated by N-acetylcysteine due to attenuated mitochondrial-derived ROS accumulation-induced endoplasmic reticulum stress, Cell Death Dis. 9 (5) (2018) 568.
[44] Q. Zhang, D. Li, X. Dong, X. Zhang, J. Liu, L. Peng, B. Meng, Q. Hua, X. Pei, L. Zhao, X. Hu, Y. Zhang, Z. Pan, Y. Lu, B. Yang, LncDACH1 promotes mitochondrial oxidative stress of cardiomyocytes by interacting with sirtuin3 and aggravates diabetic cardiomyopathy, Sci. China Life Sci. 65 (6) (2022) 1198–1212.
[45] H. Luo, R. Zhang, J. Krigman, A. McAdams, S. Ozgen, N. Sun, A healthy heart and a healthy brain: looking at mitophagy, Front. Cell Dev. Biol. 8 (2020) 294.
[46] J. Hu, Y. Zhang, X. Jiang, H. Zhang, Z. Gao, Y. Li, R. Fu, L. Li, J. Li, H. Cui, N. Gao, ROS-mediated activation and mitochondrial translocation of CaMKII contributes to Drp1-dependent mitochondrial fission and apoptosis in triple-negative breast cancer cells by isorhamnetin and chloroquine, J. Exp. Clin. Cancer Res. 38 (1) (2019) 225.
[47] M. Bonora, M.R. Wieckowski, D.A. Sinclair, G. Kroemer, P. Pinton, L. Galluzzi, Targeting mitochondria for cardiovascular disorders: therapeutic potential and obstacles, Nat. Rev. Cardiol. 16 (1) (2019) 33–55.
[48] S. Pickles, P. Vigié, R.J. Youle, Mitophagy and quality control mechanisms in mitochondrial maintenance, Curr. Biol. 28 (4) (2018) R170–r185.
[49] W.J. Liang, B. Gustafsson, Å, the aging heart: mitophagy at the center of rejuvenation, Front. Cardiovasc. Med. 7 (2020) 18.
[50] A. Shirakabe, Y. Ikeda, S. Sciarretta, D.K. Zablocki, J. Sadoshima, Aging and autophagy in the heart, Circ. Res. 118 (10) (2016) 1563–1576.
[51] A. Schiavi, S. Maglioni, K. Palikaras, A. Shaik, F. Strappazzon, V. Brinkmann, A. Torgovnick, N. Castelein, S. De Henau, B.P. Braeckman, F. Cecconi, N. Tavernarakis, N. Ventura, Iron-starvation-induced mitophagy mediates lifespan extension upon mitochondrial stress in C. elegans, Curr. Biol. 25 (14) (2015) 1810–1822.
[52] C. Vásquez-Trincado, I. García-Carvajal, C. Pennanen, V. Parra, J.A. Hill, B. A. Rothermel, S. Lavandero, Mitochondrial dynamics, mitophagy and cardiovascular disease, J. Physiol. 594 (3) (2016) 509–525.
[53] J.W. Harper, A. Ordureau, J.M. Heo, Building and decoding ubiquitin chains for mitophagy, Nat. Rev. Mol. Cell Biol. 19 (2) (2018) 93–108.
[54] A. Eiyama, K. Okamoto, PINK1/Parkin-mediated mitophagy in mammalian cells, Curr. Opin. Cell Biol. 33 (2015) 95–101.
[55] U.A. Mukherjee, S.B. Ong, S.G. Ong, D.J. Hausenloy, Parkinson's disease proteins: novel mitochondrial targets for cardioprotection, Pharmacol. Ther. 156 (2015) 34–43.
[56] B. Wang, J. Nie, L. Wu, Y. Hu, Z. Wen, L. Dong, M.H. Zou, C. Chen, D.W. Wang, AMPKα2 protects against the development of heart failure by enhancing mitophagy via PINK1 phosphorylation, Circ. Res. 122 (5) (2018) 712–729.
[57] S. Wang, W. Ge, C. Harns, X. Meng, Y. Zhang, J. Ren, Ablation of toll-like receptor 4 attenuates aging-induced myocardial remodeling and contractile dysfunction through NCoRI-HDAC1-mediated regulation of autophagy, J. Mol. Cell. Cardiol. 119 (2018) 40–50.
[58] A. Picca, R. Calvani, H.J. Coelho-Júnior, E. Marzetti, Mitophagy: at the heart of mitochondrial quality control in cardiac aging and frailty, Exp. Gerontol. 153 (2021), 111508.
[59] H.M. Li, X. Liu, Z.Y. Meng, L. Wang, L.M. Zhao, H. Chen, Z.X. Wang, H. Cui, X. Q. Tang, X.H. Li, W.N. Han, X. Bai, Y. Lin, H. Liu, Y. Zhang, B.F. Yang, Kanglexin delays heart aging by promoting mitophagy, Acta Pharmacol. Sin. 43 (3) (2022) 613–623.
[60] W. Liang, A.G. Moyzis, M.A. Lampert, R.Y. Diao, R.H. Najor, B. Gustafsson, Å, Aging is associated with a decline in Atg9b-mediated autophagosome formation and appearance of enlarged mitochondria in the heart, Aging Cell 19 (8) (2020), e13187.
[61] W. Man, J. Gu, B. Wang, M. Zhang, J. Hu, J. Lin, D. Sun, Z. Xiong, X. Gu, K. Hao, B. Guo, G. Wei, L. Zhang, R. Song, C. Li, H. Wang, D. Sun, SHANK3 Co-ordinately regulates autophagy and apoptosis in myocardial infarction, Front. Physiol. 11 (2020) 1082.
[62] A. Mattiazzi, R.A. Bassani, A.L. Escobar, J. Palomeque, C.A. Valverde, M. Vila Petroff, D.M. Bers, Chasing cardiac physiology and pathology down the CaMKII cascade, Am. J. Physiol. Heart Circ. Physiol. 308 (10) (2015) H1177–H1191.
[63] Y.Y. Wang, R. Zhao, H. Zhe, The emerging role of CaMKII in cancer, Oncotarget 6 (14) (2015) 11725–11734.
[64] S.C. da Silva Rosa, M.D. Martens, J.T. Field, L. Nguyen, S.M. Kereliuk, Y. Hai, D. Chapman, W. Diehl-Jones, M. Aliani, A.R. West, J. Thliveris, S. Ghavami, C. Rampitsch, V.W. Dolinsky, J.W. Gordon, BNIP3L/Nix-induced mitochondrial fission, mitophagy, and impaired myocyte glucose uptake are abrogated by PRKA/PKA phosphorylation, Autophagy 17 (9) (2021) 2257–2272.
[65] M. Chen, Z. Chen, Y. Wang, Z. Tan, C. Zhu, Y. Li, Z. Han, L. Chen, R. Gao, L. Liu, Q. Chen, Mitophagy receptor FUNDC1 regulates mitochondrial dynamics and mitophagy, Autophagy 12 (4) (2016) 689–702.

[66] J. Beckendorf, M.M.G. van den Hoogenhof, J. Backs, Physiological and unappreciated roles of CaMKII in the heart, Basic Res. Cardiol. 113 (4) (2018) 29.
[67] M.L. Joiner, O.M. Koval, J. Li, B.J. He, C. Allamargot, Z. Gao, E.D. Luczak, D. D. Hall, B.D. Fink, B. Chen, J. Yang, S.A. Moore, T.D. Scholz, S. Strack, P.J. Mohler, W.I. Sivitz, L.S. Song, M.E. Anderson, CaMKII determines mitochondrial stress responses in heart, Nature 491 (7423) (2012) 269–273.
[68] E.D. Luczak, Y. Wu, J.M. Granger, M.A. Joiner, N.R. Wilson, A. Gupta, P. Umapathi, K.R. Murphy, O.E. Reyes Gaido, A. Sabet, E. Corradini, W.W. Tseng, Y. Wang, A.J.R. Heck, A.C. Wei, R.G. Weiss, M.E. Anderson, Mitochondrial CaMKII causes adverse metabolic reprogramming and dilated cardiomyopathy, Nat. Commun. 11 (1) (2020) 4416.